

We are IntechOpen, the world's leading publisher of Open Access books Built by scientists, for scientists

6,900

Open access books available

185,000

International authors and editors

200M

Downloads

Our authors are among the

154

Countries delivered to

TOP 1%

most cited scientists

12.2%

Contributors from top 500 universities



WEB OF SCIENCE™

Selection of our books indexed in the Book Citation Index
in Web of Science™ Core Collection (BKCI)

Interested in publishing with us?
Contact book.department@intechopen.com

Numbers displayed above are based on latest data collected.
For more information visit www.intechopen.com



Some Features of Growing Single Crystals of Refractory Metals from the Melt

Vadim Glebovsky

Additional information is available at the end of the chapter

<http://dx.doi.org/10.5772/59651>

1. Introduction

Mostly single crystals of semiconductors, dielectrics, metals, or alloys are produced in the process of crystallization or solidification from the melt. The rates of crystallization can reach tens of millimeters per minute. During crystallization in single crystals, structural defects can be collected, that have a negative effect on the mechanical and other properties of materials. High demands for structural perfection and chemical purity of single crystals caused considerable research efforts aimed at the study and improvement of the main techniques of growing single crystals from the melt (Czochralski, Stepanov, Bridgman, Verneuil, floating zone). Single crystals of refractory *bcc* metals, especially molybdenum and tungsten, are widely used in several areas of modern technology, such as nuclear energy, electronics, lighting fixtures, mainly for the manufacture of parts and devices (anodes, cathodes, *etc.*) working at high temperatures. A scope of single crystals of refractory metals is continuously expanding, and requirements for chemical purity of crystals, their structural quality and geometry are constantly growing. Currently, the most pure single crystals of molybdenum and tungsten, as well of a number of other refractory metals can be produced by electron-beam floating zone melting (EBFZM). However, their crystallographic perfection due to the specific features of the floating zone method with electron-beam heating, often no longer satisfies the developers of new instruments and devices. A characteristic blocky structure and a high density of dislocations make such crystals unsuitable, for example, for research of channeling high-energy particles or posing a number of other subtle physical experiments. Further increase in a degree of purity and crystallographic perfection of single crystals of refractory metals is closely related to a development of theoretical and experimental researches of crystallization processes, the development of new apparatuses and methods for producing single crystals, as well as optimization of known processes. Therefore, to obtain additional information about

the laws of formation of a dislocation structure, an impact on specific parameters of crystal growth in the floating zone method seems to be relevant scientific and technical challenge. The basis of this decision is a study of peculiarities of structural defects in single crystals grown by crystallization, which is one of the fundamental problems of solid state physics, physical chemistry, and theory of phase transitions.

2. Basic physical features of crystallization

2.1. Methods of growing single crystals from the melt

For growing oriented single crystals of semiconductors and dielectrics Czochralski method became widespread [1-3]. The essence of the method consists in pulling of single crystals by seeding at a surface of the melt. Although this method of capillary formation is known by its low stability, at high precision heating control and automation of pulling [4-6] it allows obtaining such semiconductors as silicon and germanium which are widely used in modern technology. Bridgman method, which also refers to the crucible methods similar to Czochralski, is used in a much smaller scale and mostly for growing single crystals of low-temperature melting metals. This is due to the fact that at high temperatures there are significant difficulties in finding materials for crucibles. Another widely used technique is Stepanov method of growing single crystals. Its difference from Czochralski consists in that the shaper is immersed into the melt, providing not only pulling cylindrical rods, but also production of a wide assortment of shaped crystals (tapes, tubes, polyhedrons, and other crystals of a complex shape). Stepanov method has much greater margins of stability during capillary shaping than Czochralski, which accounts for its wide distribution. However, for growing single crystals of refractory metals, especially molybdenum and tungsten, the above-mentioned methods are not suitable, as the high melting temperature and high chemical reactivity of liquid refractory metals do not allow obtaining them by any crucible method. The actual process of the growth is desirable to maintain in a vacuum or in an inert gas. For refractory metals Verneuil method is also used provided with another kind of a heater as plasma. This method yielded the most by large-scale tungsten single crystals of 40 mm in diameter and weighing up to 10 kg [7]. However, those single crystals were of poor structural quality and had high gas content, especially of a plasma gas. The most perfect single crystals of refractory metals can be obtained by electron-beam floating zone melting. The growth of these crystals is characterized by the fact that the method is a crucible-less one and a melt has no any contact with other materials. The melt is supported by forces of surface tension and the process is carried out in UHV. A phase diagram can give information on the type, number and volume fraction of phases at crystal growing from the melt [8]. This is true only in the case when crystallization proceeds at an infinitesimal rate. In practice, a finite rate and solidification conditions are far from thermodynamic equilibrium. Thus, binary alloy solidification occurs with enrichment or depletion of solid with a dissolved component. When impurity accumulation exceeds some critical value and a temperature gradient in liquid is reduced below a critical level, there comes concentration supercooling and the interphase surface changes from cellular to dendritic. This is nonequilibrium solidification and is typical of most alloys. A main feature of such solidifi-

cation is that a primary axis of dendrites is strictly parallel to a heat flow direction and interdendritic spaces are enriched with impurities. This segregation further can be partially eliminated by prolonged high-temperature annealing. In some cases, there may be precipitates of a second phase in interdendritic spaces. When crystal growth conditions are such that a part of a two-phase zone is large and a growth rate is high, so that the factor is a lot less than zero: $G - V(FR)_{eff}(1/D) \ll 0$, where, G the temperature gradient in fluid; V the growth rate; $(FR)_{eff}$ the effective solidification range; D the diffusion coefficient. Thus, there is a porosity which may occur even in growing single crystals of pure refractory metals by EBFZM. It occurs especially after the first liquid zone passage during purifying the initial PM feed and growing a single crystal from. EBFZM provides not only a given orientation of crystal growth, but also due to refining by a zone effect mainly from substitution impurities. Refining of interstitial impurities occurs mainly by vacuum evaporation, the more that the melting points of refractory metals are very high. Impurities in a growing crystal often are undesirable as adversely affecting its structure and properties. In the process of accumulation of impurities before moving crystallization front, the plane crystallization front may become unstable due to so-called phenomenon of concentration supercooling. Impurities will greatly impair the dislocation substructure and unevenly distributed in a radial direction and a length of the crystal along the growth axis.

2.2. Mechanisms of crystallization of metals

Crystallization processes are widely used in modern science and technology: the growth of single crystals, production of pure substances by directional crystallization and zone melting. Crystallization in metallurgy - is one of the stages of producing metals, such as crystallization in molds, continuous casting, and processes in molds during refining. Currently, by theory of crystallization the following molecular mechanisms of the crystal growth are developed: nucleus, spiral, normal, continuous [1,2]. The crystal growth by two-dimensional nucleation leads to an expression for the growth rate:

$$v = C \exp(-U/kT) \exp(-A/kT), \quad (1)$$

where, A the work of two-dimensional nucleation; U the activation energy of the atom addition to the brink of the nuclei; C the kinetic coefficient, which is first analyzed in [9,10]. It should be noted that much more other growth mechanisms implemented. Thus, the crystals containing dislocations cannot be grown by two-dimensional nucleation. A spiral stage formed near an exit of the dislocation on the crystal surface plays a role of non-vanishing two-dimensional nucleation, which facilitates the connection of new particles to the crystal. This theory gives an expression for the crystal growth rate in the following form [2]: $v = DL \Delta T / 4\pi r T_0^2$, where, D the diffusion coefficient; ΔT the supercooling; L the heat of crystallization; T_0 the melting point. Two-face growth mechanisms in a tangential direction are implemented in practice. A condition for the growth by these mechanisms is the presence of an atomically smooth surface that holds only for substances with high heat of fusion and areas with low crystallographic indices. Crystals with low heat of fusion, which include almost all metals, have atomically

rough edges; their micro relief varies continuously over time. Micro fluctuations of the atomic structure of the interface lead to active participation of all points on the surface of the crystal, and for all metals $L/kT_0 < 2$. Thus, metals are characterized by a normal growth mechanism. This mechanism is used for all values of supercooling, and specifically in the field of small deviations from equilibrium state of the system it becomes predominant. A normal mechanism is related to thermal fluctuations at the interface and therefore has greater sensitivity to small differences in temperature. According to theory of continuous growth, crystals in the neighborhood of equilibrium can grow exclusively through nucleation at the interface. Disadvantage of this theory is neglecting thermal fluctuations of the equilibrium type on the interphase between solid and liquid phases. This leads to the fact that the growth rate is described by quadratic or exponential functions which is characteristic of classical theories. Considered mechanisms of the crystal growth are characteristic for most typical cases of the free growth, *i.e.*, when nothing prevents the crystal growing in either direction. However, in Czochralski and floating zone one has to deal with cases of the stimulated growth.

2.3. Heat and mass transfer processes in crystal growth from the melt

When moving the crystallization front in the melts a set of complex physical and chemical processes occur: heat transfer and mass transfer in the melt and crystal, out impurities processes and impurity redistribution at the crystallization front, capillary phenomena, and metal evaporation. Under these conditions, the most important and crucial for the structural quality of the growing crystal is the temperature gradient in the liquid and solid phases ($G = (\partial T / \partial n)_{S,L}$). Temperature gradients ($K\text{ mm}^{-1}$) occur at the crystallization front and are defined by intensity of a heat sink, chemical composition of the metal, release of crystallization heat, a heat input to the liquid metal, and convective flows in the melt [11]. In principle, stability of the crystallization process and quality of the single crystals grown are mostly influenced by the temperature field in the thermal zone of the growth set-ups, *i.e.*, the temperature field in the crystal and melt. Of particular importance are temperature conditions at the crystallization front. A heat balance at the interface looks like:

$$\lambda_L (\partial T / \partial n)_L + L\gamma v = \lambda_S (\partial T / \partial n)_S, \quad (2)$$

where, v the rate of crystallization; L the latent heat of crystallization; γ the melt density, kg m^{-3} ; λ_L , λ_S the thermal conductivity of the liquid and solid phases, $\text{W cm}^{-1} \text{K}^{-1}$; n the normal to the surface of the interface; $(\partial T / \partial n)_S$ and $(\partial T / \partial n)_L$ the temperature gradients near the crystallization front. In simplified calculations suggest the phase boundary plane and then $(\partial T / \partial n) = (\partial T / \partial z)$, which are the axial temperature gradients. The temperature field in the growing crystal also has a significant impact on its structure. The main cause of dislocations in the crystal is plastic deformation caused by thermal stresses which are typically caused by uneven cooling the crystal in the region of loss of plastic properties of material. The lower $(\partial T / \partial n)_S$ for the growing crystal, the more perfect is its structure; a low value means a lower productivity of the process. Indeed, if we take $(\partial T / \partial n)_L = 0$, we obtain:

$$v_{max} = (\lambda_S / L\gamma) (\partial T / \partial n)_S, \quad (3)$$

Now, if we assume that a heat transfer from the surface of the crystal is carried out mainly by radiation, we obtain:

$$v_{max} = (1 / L\gamma) \sqrt{4\lambda_S \sigma_0 \varepsilon T_0^5 / 3d_0}. \quad (4)$$

Where, T_0 the crystallization temperature, K; $\sigma_0 = 5.67 \times 10^{-12}$, W cm⁻² K⁴, the Stefan-Boltzmann constant; ε the emissivity of surface radiation of the crystal; d_0 the crystal diameter, cm. A significant impact on the structure of the growing single crystal has a shape of the interface crystal-melt, which can be considered as the isothermal surface having a temperature of solidification. The most favorable form of the crystallization front is flat or somewhat convex to the melt [12,13]. This reduces the number of defects formed and contributes to their more uniform distribution in the crystal. For example, dislocation-free silicon single crystals are grown under the conditions of the crystallization front of forms close to a plane. The power needed to produce a molten zone of a predetermined shape is studied using a simplified model [14]. It is shown that Laplace's equation can describe the temperature changes along the rod and in the zone with a help of numerical methods. It is also found that the temperature distribution is characterized by several dimensionless Biot numbers, representing the ratio of the thermal conductivities in the liquid and solid phases, ratio between the length of the rod and width of the molten zone along the radius of the crystal, and power. The resulting temperature distribution and forms of the liquid zone for different Biot numbers and coefficients of thermal conductivity obtained as functions of the energy supplied to the zone. A horizontality of isotherms near the solidification front decreases the radial gradient and thus stabilizes the axial gradient $(\partial T / \partial n)$. As for the value of the latter, on this account, there are conflicting opinions. On the one hand, increased $(\partial T / \partial z)_L$ near the phase boundary promotes better ousting impurities, improve stability of the crystallization process, increase the growth rate, reducing a likelihood of spontaneous crystallization due to concentration supercooling. On the other hand, excessive $(\partial T / \partial z)_L$ at the interface causes increasing convective flows; this can lead to uncontrolled temperature fluctuations near the crystallization front. The latter circumstance causes a very common defect in crystals – a streaky micro inhomogeneity of impurities [15]. In addition to the temperature distribution near the crystallization front in the vicinity of the phase boundary, the temperature field is also important in a whole volume of the melt, as a prerequisite exception of spontaneous crystallization is overheating the melt outside the phase boundary. The temperature field in the entire volume of the melt determines existing natural convection flows. It is also important obtaining an axial symmetry of the temperature field. When growing semiconductors, it is necessary to reproduce temperature gradients with accuracy of $\pm 0.5^\circ$ C cm⁻¹ in certain areas of the thermal processing zone. Of particular note is the fact that the temperature field in the crystal and in the melt cannot be considered outside the context of each other. Adjustment of the temperature field in the crystal will cause changes of the temperature field in the melt (opposite is also true). This makes it difficult to control when growing. The technological practice (primarily for growing semicon-

ductor crystals) shows that for high-quality single crystals with desired properties it is necessary to accurately maintain the set of the temperature mode in time. A tough time maintaining the temperature field should be of the high-precision and high-rate automatic control system. The most important is to maintain the constant temperature in time at the crystallization front. The main factors disturbing the thermal regime are oscillations of the power input and fluctuations of the heat loss. The latter means impermanence of the cooling water to elements of a design as well a variable heat removal through the growing crystal. In some cases, to eliminate disturbances associated with a change in internal conditions it is necessary to make corrections in advance by changing the computer programmed temperature. In this case allowable temperature fluctuations in obtaining perfect semiconductor crystals should not exceed 0.1°C . Instabilities of the temperature lead to the increased dislocations density, but in some cases of more serious defects (twins, portions of the polycrystalline structure, *etc.*). In addition, the structural quality of single crystals affects by the rate of the zone movement and its fluctuations. With increase in the rate, the dislocation density is greatly increased. This limit for niobium is of 0.5 mm min^{-1} . From perspectives of influence on the structure, the zone movement rate must be stable up to about 1%, and all kinds of vibration should be excluded.

2.4. Influence of convection in the melt on the crystal structure

In recent years, an interest has grown significantly to convective phenomena in the melt during the growth of single crystals. In particular, this is due to the possibility of conducting experiments in space. A large number of studies on convection in the melt during the growth of single crystals were done by various methods. Hydrodynamic phenomena are typical of the floating zone method [13-15]. It should be noted that phenomena of convection are studied by two ways: convective phenomena experimentally investigated by physical modeling of the crystal growth in transparent liquids and by constructing mathematical and computer models. Mathematical models tend to represent a complex system of differential equations. Main assumptions in constructing models are stationary, two-dimensional and axisymmetric of the hydrodynamic problem [13]. Characteristic of models is the extensive use of dimensionless criteria of similarity theory. Particular attention is paid to thermocapillary convection (Marangoni convection) [15]. Results of model experiments and calculations are used to explain some properties of single crystals of molybdenum, so that study is considered in more detail. Convective flows in the melt can have a significant impact on the structure and properties of the growing single crystal. Important parameters such as impurities and the concentration and temperature gradients in the melt are dependent on nature of flows. The shape of the crystal-melt interface appears to depend not only on heat transfer processes, but also on conditions of the melt flows. Consider the most important similarity criteria which give a relation between the convective and diffusive heat and mass transfer. It is accordingly Prandtl $Pr = \theta/\varphi$ and Schmidt $Sc = \theta/D$, where θ the kinematic viscosity of the melt; D the diffusion coefficient; φ the thermal diffusivity. For typical metallic melts $Pr \ll 1$, $Sc \gg 1$, *i.e.*, the heat transfer occurs mainly by conduction, and the impurity transfer occurs by convection which plays a significant role. Therefore, it can be expected that microsegregation in the crystal melt is associated with hydrodynamics of the melt. The experiments were done by EBFZM of molybdenum with

additives of iridium-192 ($K_0 = 0.37$) and tungsten ($K_0 = 50$). X-ray topograms and autoradiograms of longitudinal cross-sections of samples showed characteristic bands enriched with impurities. If we assume that the melt is the incompressible fluid, the density of which depends on the temperature and impurity content, the forces, that give rise to convective flows in the melt, are the following: gravitational forces (cause natural convection), capillary forces (cause Marangoni convection) and inertial forces (occur when the crystal is rotated). In general, flow patterns in the molten zone are the result of the joint effect of these forces. Before discussing the problem of convection we should consider features of the temperature distribution in the molten zone. The interfacial crystal-melt surface at the crystallization front has a temperature T_0 . The maximum temperature $T_0 + \Delta T$ is in the middle of the zone, *i.e.*, there is the positive axial temperature gradient. Furthermore, there is the negative radial gradient directed from the periphery toward the center of the zone. Arising under these conditions vertical density gradients, causing steady natural convection, can be described by Rayleigh numbers $Ra = \alpha g \Delta T h^3 / \nu \varphi \sim 10^3$, where, g the acceleration due to gravity; α the coefficient of thermal expansion; h the half a zone length. As for radial temperature gradients, they correspond to Rayleigh numbers, almost equal to zero. Acting on the free surface of the melt the surface tension forces are functions of temperature, $\sigma = f(T)$. If on the free melt surface the temperature gradient exists, resulting in changes in surface energy, then capillary Marangoni forces begin to act. These forces give rise to characteristic convection in the melt. The rate of flows caused by Marangoni forces is greatest at the surface of the melt. With increasing the distance from the surface the rate decreases and then changes its sign. In the case of the zone melting Marangoni forces act on the periphery of the zone from its middle to interphase boundaries. The power of Marangoni forces is characterized by Marangoni numbers $Ma = |\partial\sigma/\partial T| (\Delta T h^2 / \rho \nu \varphi)$, where, $|\partial\sigma/\partial T|$ is the temperature coefficient of surface tension; ρ the density of the melt. The ratio of Rayleigh number to Marangoni number characterizes the ratio of forces of free convection and Marangoni convection: $Bo = Ra / Ma = g \rho \alpha h^2 / |\partial\sigma/\partial T|$. When $Bo < 1$, Marangoni flow dominates in the melt. It takes place in normal gravity when $h \leq 1$ cm [15]. In the absence of rotation, Marangoni flow in the melt is toroidal axially symmetric. With increasing Bo outer vortices increasingly dominate over the lower ones. This leads to the non-uniform transfer of impurities in the melt and eventually to the radial non-uniformity of impurities. Increase in the dislocation density in the crystal can be explained by the interfacial surface curvature produced by convection. At $Ma > 3.4 \times 10^3$ flows become unstable. There are variations in the temperature within the melt with a frequency $f \sim h^{-1} d^{-1}$, where d is the diameter of the crystal. This leads to such defects in the crystal as impurity bands which is found at the respective longitudinal sections of the X-ray topographs [15]. The width of the bands associated with the zone and the rate of the oscillation frequency $f: a = v / f$, where, v is the growth rate; a is the width of the band. Temperature fluctuations lead to reduction of K_{eff} and further to macrosegregation. The banded heterogeneity may disappear at growth rates below a certain critical value due to fairly good diffusion in the solid phase. We must also mention the detected submicroporosity in molybdenum single crystals grown by EBFZM after the first and second zone runs. These submicropores of diameter 0.3-0.5 micron decorate the interphase boundary and are also associated with temperature oscillation, because arranged by bands and seen on cleaved samples in scanning electron microscope.

2.5. Thermal stresses and dislocation structure of single crystals

For the first time in 1958, Dash [16] has grown dislocation-free silicon single crystals from the melt using the method of a narrow waist or a neck. He believed that dislocations appeared from the seed in the waist region, come to the surface, and stresses, occurring during further growth, cannot generate dislocations, if initially they did not exist in the crystal. Since dislocation defects are non-equilibrium, they may only be a consequence of non-equilibrium growth conditions. According to [1,2,15], for the formation of dislocations are responsible: external stresses of mechanical origin; thermal stresses; local stresses due to concentration gradients; condensation of vacancies; local stresses due to inclusions; errors during growth. Thermal stresses, occurring during the growth of single crystals from the melt, lead to significant increase in the dislocation density. Application of dislocation theory and theory of internal stresses to the problem of the crystal growth has led to significant achievements. It is shown that the main source of stresses causing deformation and dislocation multiplication in the growing crystal is the inhomogeneous temperature field. Thus, in the case of growing the single crystal of the radius R by crystallization from the melt, the following estimate for an absolute value arising from thermal stresses in the crystal: $\tau = k\alpha ER^2 T_z''$, where, α is the coefficient of linear expansion; k is the coefficient; E is the Young's modulus; R is the radius of the crystal; T_z'' is the second derivative of the temperature by a coordinate z . From this it follows that the crystal growth is necessary to strive to ensure that the temperature field in the growing crystal should be as close as possible to the linear one, so T_z'' would be minimal. A number of experiments in growing single crystals of germanium show that in a case of active shielding (heated screens) it was succeeded by significantly reduce of the amount of T_z'' down to values of an order of 0.05 K mm^{-2} . Due to this, the dislocation density has been reduced by almost two orders of magnitude. Admissible a following upper estimate for the density of dislocations arising from thermal stresses: $\rho \geq \alpha \text{ grad}T / b$, where, α is the coefficient of thermal expansion; b is the Burgers vector. Note that growing single crystals of metals with the low dislocation density is significantly harder than single crystals of semiconductors or dielectrics. This is due to the fact that elastic constants of metals go to zero much faster as the temperature approaches the melting point [9,10]. The structural perfection of single crystals grown from the melt is influenced not only by the temperature gradients themselves, but the important factor in this respect is the cooling rate which is implemented at the stage of the crystal growth itself, and then under cooling to room temperature [17]. An influence of growth conditions on the dislocation substructure of copper single crystals is investigated in [18]. At a regular control of the dislocation structure, the Cu[111] single crystals are grown from the melt at the rate of $0.2\text{-}120 \text{ mm min}^{-1}$. Variation of the growth rate in this range had a little effect on the random growth of the dislocation density inside subgrains which was $\sim 2 \times 10^6 \text{ cm}^{-2}$. With an increase in the growth rate an average size of subgrains is significantly reduced from $5 \times 10^{-2} \text{ cm}$ to $0.5 \times 10^{-2} \text{ cm}$, and this decline is roughly proportional to the cooling rate of the crystal rising -0.5 in accordance with the model of the dislocation origin of sub-boundaries. On the basis of these experiments, the conclusion is made that the model of the sub-boundaries formation is valid, and impurities do not play any significant role in the formation of the substructure in copper single crystals of purity less than 99.999%.

3. Experimental

3.1. The set-ups for electron beam floating zone melting

History of the development of EBFZM method to produce refractory metals in the single-crystal form has more than seventy years [19,20]. Over the past thirty years there was a significant progress both in improving experimental techniques used for growing single crystals of refractory metals, and the study of their structure and properties. However, even the well-known and successful designs of the electron gun [19] and EBFZM set-ups did not allowed to conduct a lengthy process of growing and were “not-easy” to operate. Then, the most advanced electron-beam guns are presented in [21-24]. There have been developed and tested the original EBFZM set-ups for growing single crystals of refractory metals. In the design of these set-ups have been successfully resolved the main problems concerning the mechanisms of the movement of the cathode assembly, the electron gun, the power supply and others (Figure 1). Single crystals, bicrystals and tubular crystal of many transition and refractory metals were grown using the electron guns with the protected annular filament-cathode in EBFZM set-ups.

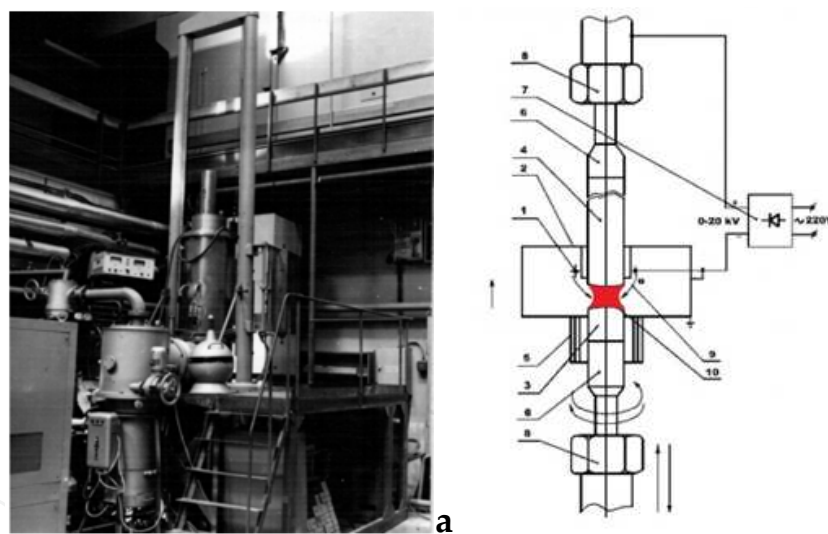


Figure 1. EBFZM set-up (a) and scheme of a thermal zone (b).

A principle of operation of EBFZM set-ups with annular electron guns, in a certain extent, is similar to a function of the vacuum triode: the tungsten filament (cathode), the feed sample (anode), focusing electrodes (control grid), the melting chamber (housing). The voltage, current and power, which are consumed for melting the feed, refining the liquid metal and growing the single crystal, are determined not only by both the anode voltage and the current of the cathode filament, but also by the residual gas pressure in the cathode-anode gap. In EBFZM set-ups for operation of the electron gun is very important the gas release from the feed during melting. Any sudden rise in pressure due to the gas release, metal evaporation or local vacuum decay even to 10^{-1} Pa in the electron gun lead to avalanche of a low resistance of

the anode-cathode system and even to complete destabilization of the electron gun. From the above there are basic requirements to EBFZM set-ups providing conditions for the stable zone melting: stability of the electron gun; stability of the power supply; perfection of moveable nodes; an impurity homogeneity of the feed, otherwise it can cause unpredictable sharp increase in pressure in the melting chamber. It should be noted that the most sensitive element of EBFZM set-ups is the electron gun, so the focus of this section will be paid to the designs of electron guns, which should create the optimal and stable over time temperature field. Electron guns in many EBFZM set-ups have some disadvantages that prevented widespread of the method and demanded a lot of efforts to correct them. Typically, the designs of all known guns are such that spatters and vapors of metal get to the cathode filament, thereby destabilizing functions of the gun, changing its power due to local decrease in emissivity of the cathode filament. This often leads to burnout of the cathode and to finish the growing process. Another disadvantage of existing electron guns is contamination of the feed and crystal by metal vapors from which the cathode is made (usually tungsten), and the electron gun itself. Such contamination is most likely when the cathode is located in "line of sight" visibility of the feed, which is typical for almost all designs of electron guns. At 2500K the rate of evaporation of tungsten is less than $2 \times 10^{-10} \text{ g s}^{-1} \text{ cm}^{-2}$ and thermionic tungsten cathodes are sufficient to melt all metals. Three-electrode electron guns with a single accelerating electrode allow to stabilize power supplied to the zone and to eliminate variations of the temperature during the growing process. It was also assumed that accelerating electrodes could act as modulators of the anode current, which would maintain without inertia the given heat regime and have significant advantages compared with known control systems. Naturally, electron guns, in which the upper and lower borders of focusing are realized by mechanical devices, do not meet these requirements.

Benefits of both EBFZM set-ups and electron guns [20] compared to previous ones consisted in the fact that metal vapors and spatters cannot reach the cathode and the liquid zone because the cathode filament is outside of a "line of sight". Main criteria for using new guns in EBFZM set-ups are: simplicity of the design, as well as reliability of operation at high temperatures and intensive sputtering. The density of the electron flux from the filament (with the current leads nearby) is for 3-5 times higher as compared with the opposite side of the same filament (without the current leads nearby). Such asymmetry of electron fluxes is observed in all guns in which the ring filament is made of two semi-rings. The asymmetric distribution of the electron density causes an asymmetry of the temperature field in the liquid zone and, as a result, the asymmetry of heating of the growing crystal. By the way, this may be one of reasons for the "snap" growth of single crystals. Apparently, the heterogeneous structure, which is characterized by a layered distribution of both impurities and defects, is a consequence of a mismatch of the thermal axis and the axis of the growing crystal. One of the main practical conclusions is that, despite an apparent lack of difference between one- and two-element cathodes, only a singleton cathode in the form of the loop provides satisfactory symmetry of the electron flux and temperature field. It contributes to the problem of obtaining homogeneous single crystals with the reproducible structure and crystallographic characteristics along the entire length. The basic requirements that determine conditions for the stable operation of the electronic guns and, especially, EBFZM set-ups can be formulated as follows: an absence

of sputter on the filament, *i.e.*, the filament should be in the "shadow", and the system of focusing electrodes should provide the appropriate curvilinear electron beam and focus it on the sample-anode; the design of the electron gun should ensure a prompt removal from the inter-electrode space all gases released from the sample; the gun design must give certain rigidity and total absence of warping after the prolonged exposure to high temperatures, so all the parts of the gun must be performed of a high thermal conductivity material (*e.g.*, copper) and cooled by water; high vacuum EBFZM set-ups should be met by the tightness of the melting chamber, the pumping powerful vacuum system and reduced gas release from samples; the power supply must provide a long-term operation of the annular electron gun at given electric modes; moving both the annular electron gun and sample-anode during growing should be coaxial at the whole length of the sample [20,21]. Figure 1b shows a schematic interior of EBFZM set-up for growing crystals and bicrystals. The liquid zone 10 on the single-crystalline rod 4 is produced by the electron beam 9 emitted from the tungsten filament (cathode) 1. Focusing is carried out by the electron gun 2. The power supply provides the accelerating voltage of 25 kV and the anode current up to 1 A. The growth rate of bicrystals is $1\div 1.5 \text{ mm min}^{-1}$ while rotating the seed 6 at the rate 20 rev min^{-1} . A lack of positive feedbacks between the cathode and the anode in the electron gun allows maintaining the average power of the electron beam, which is almost constant throughout the growing single crystals or bicrystals. Random power fluctuations with a frequency of several hertz do not exceed 0.1% of a nominal value.

3.2. Metallographic examinations

Metallographic examinations of the crystal structure at the macro and micro levels provide extensive qualitative and quantitative information about the structure [22-24]. A possibility exists to measure of various structural elements up to 1 micron. A range of crystallographic planes of the crystal orientation can be determined by etch pits and execute it with an accuracy of $\pm 3\div 5^\circ$. The dislocation density in the crystal can be evaluated according to the number of etch pits per unit area (in the event that it does not exceed 10^8 cm^{-2}). An interference attachment to a metallographic microscope gives a possibility to evaluate the surface roughness of cross-sections. The polarization console allows detecting inclusions of the second phase in a sample, if the latter is present in significant amounts. To carry out metallographic studies the sample must first be cut off from the corresponding bulk single crystal and then prepared by grinding. Cutting samples of molybdenum and tungsten single crystals of necessary geometry and crystallographic orientations can be produced by the electroerosion device. It is well known that this technique can produce a significant damage of the sample surface - to a depth of about 300 microns. When this happens, the surface contamination and defects lead to increase of dislocations in the surface layer, but also there appear a typical network of cracks extending to a considerable depth. After cutting, all the above defects must be removed by both the mechanical grinding and polishing. Then, the cold-worked layer should be removed by chemical etching and electropolishing at the optimal conditions. However, it is necessary to keep in mind two things. First, all etchants are divided into two large groups. The first group has a pronounced orientation effect, *i.e.*, gives well-cut pits that are useful for determining an orientation of the crystal. In general, the etching figures revealed by these etchants have

nothing with the outgrowth of dislocations. The second group represent etchants to produce etch pits, revealing the outgrowing low-angle boundaries and individual dislocations. But even in this case to speak about one correspondence of etch pits and dislocation is not correct, it requires evidences in each case. With regard to detection of the microstructure of tungsten and molybdenum crystals is, for example, a commonly known Murakami etchant (10 g NaOH, 30 g of $K_3Fe(CN)_6$, 100 g of H_2O) which has a strong orientation effect, although it is also identifies some low-angle boundaries. Electrochemical etching in a 5% aqueous solution H_4OH gives similar results as Murakami etchant. In our view, it is more convenient to identify the substructure of the molybdenum and tungsten single crystals by an electrolytic etching in 25% NH_4OH solution under the following conditions: the current density $j = 5\div 10 \text{ mA cm}^{-2}$, the voltage $U = 2\div 3 \text{ V}$ and the time $\tau = 60\div 90 \text{ s}$. It turns out that the etchant "works" not only to identify dislocations, but also to reveal dislocations introduced into the crystal as a result of plastic deformation at the surface with a prick of the diamond indenter. Furthermore, this etchant identifies sub-boundaries with small misorientation angles and thus it has been widely used to detect the substructure of molybdenum and tungsten single crystals, grown from the melt by EBFZM. For metallographic studies the optical microscopes and automatic analyzer are used. The latter is widely used for the quantitative metallographic analysis of the linear substructure: the subgrain size distribution along and across the crystal, the dislocation density inside the subgrains averaged at least for 20 fields of view, and by the stereometric metallographic analysis as well. It should be noted that at identification of the subgrain structure of molybdenum and tungsten single crystals by means of the above proposed etchants, the metallographic studies are possible mainly at the planes of low crystallographic indices of the type $\{001\}$ and $\{111\}$ planes as well as with higher indices deviate from these planes in opposite directions at angles in the range $10\div 15^\circ$.

3.3. X-ray studies

It is known that in many cases some low-angle boundaries can be qualitatively compared by misorientation angles. In other words, it is a qualitative determination, where misorientation angles of neighboring subgrains are more and where – less, because a quantitative determination of misorientation angles by metallographic methods is impossible. To obtain such information on the real structure of the crystal it is necessary to use methods of X-ray diffraction microscopy. Here, to obtain the quantitative information about misorientation angles of the substructure elements of molybdenum and tungsten single crystals we used both the X-ray topograms of angular scanning and X-ray recording by the wide divergent beam. Especially clear for determining misorientation angles is the method of the X-ray wide divergent beam [25]. On the X-ray record of the perfect crystal, free of low-angle boundaries, Kossel lines are solid curves of the second order. In the block crystal, recording through the low-angle boundary between adjacent subgrains, the orientation changes abruptly and Kossel lines contain gaps. Both methods allow defining misorientation angles of substructure elements with a resolution of $\sim 1 \text{ arc min}$, and linear dimensions of subgrains with a resolution of about $3\div 5 \text{ microns}$. To determine the orientation of crystals and the fulfillment of their orientation in the desired crystallographic direction with an accuracy of $\pm 1\div 2^\circ$ was used as the standard method of taking Laue epigrams.

3.4. Electron microscopy studies

Of serious interest is the question about what kind of dislocations occurs during growth from the melt? It rises from the standpoint of a study of physical aspects of the crystallization process. Most of dislocations are assembled into grids and walls as a result of polygonization processes and form the characteristic substructure. Such dislocation ensembles consisting of growth dislocations are also of interest. To undertake such a research on the real crystal structure the most suitable method is transmission electron microscopy, which allows determining the type of dislocations, their Burgers vectors and crystallography of low-angle boundaries. However, consider the following fact: as a rule, in molybdenum and tungsten single crystals grown from the melt by zone melting, the dislocation density inside the subgrains is of a value $\rho \geq 10^5 \text{ cm}^{-2}$. By other words, an average distance between dislocations is $X \approx 0,003 \text{ cm} \approx 30 \text{ micron}$ with an average size of subgrains $d \approx 500 \text{ micron}$. It means that the volume, occupied by actual low-angle boundaries, is negligible. This also means that in the case of preparing foils for electron microscopy of an arbitrary portion of a bulk sample, a single dislocation from a subgrain volume can be observed in one of 5÷10 samples. Observation of low-angle boundaries of such samples would require at least 10 times more samples (taking into account that a really observable surface of a sample has an area of about 5 micron²). Naturally, to prepare samples having such little hope of success is a real Sisyphean task. Therefore, a method of preparation of foils is used, which provides a hole in a specified area in vicinity of low-angle boundaries. An essence of the method is as follows. On one side of the original sample in a form of the washer of diameter 3 mm and thickness of 0.3-0.4 mm the substructure is detected using metallographic techniques. Then, on this side of the sample a protective film of a clearcoat (in the simplest case – a collodion) is applied to the surface and thoroughly dried. Next by the microhardness recorder PMT-3 using a diamond indenter the protective layer is violated in the right place (or a series of injections or scratches) and by electropolishing a recess of a required depth is received. Optionally, this set of operations might be repeated. It should only be kept in mind that in the process of the electropolishing all of dislocations should be removed from the surface layer of the sample, introduced there by the action of the indenter. Thereafter, the varnish is removed from the sample surface by using an organic solvent (acetone, ether) and the electropolishing is performed from the reverse side of the sample before the formation of holes. With the described method of the sample preparation, a likelihood that low-angle boundaries would be available for observation increases substantially - to 1/5÷1/10 (an experimental evaluation).

3.5. Chemical purity

As mentioned before, the presence of significant amounts of impurities has a significant impact on the structure and properties of the crystals, and for molybdenum and tungsten the greatest impact on the properties is made by interstitial impurities, primarily carbon, which is characterized by very low solubility limits in the solid state at room temperature [26]. Therefore, the analysis of the chemical composition and purity control of single crystals is an important part of the characterization of a material. In this work, an oxygen content is determined by fast neutron activation with a sensitivity of $5 \times 10^{-5}\%$, carbon is analyzed by deuteron-activation with a sensitivity of $10^{-6}\%$ [27,28]. Additionally, carbon is monitored by the coulometric method on

AN-160 device with a sensitivity of $5 \times 10^{-4}\%$. To determine other impurities in single crystals and bicrystals, mass-spectrometry with a sensitivity of $10^{-6}\%$ is used. The content of impurities is shown in Table 1. The purity of metals is also checked by a residual resistivity at liquid-helium temperatures, since at low temperatures the main mechanism of the carriers scattering in metals is scattering on impurities [29]. Here, the ratio of resistivities at room and liquid-helium temperatures is defined by the non-contact and four-contact methods. For the single crystals studied this value is not less than $(2 \div 3) \times 10^4$.

Metal	Content of impurities, $\times 10^{-4}\%$											
	O	C	N	H	Si	Al	K	Ca	Na	P	S	Mn
Mo	<0.5	<0.5	<0.6	<1.0	<0.3	<0.1	<0.1	<0.1	<0.1	<0.03	<0.1	<0.03
W	<0.5	<1.0	<0.6	-	<0.3	<0.1	<0.1	<0.1	<0.3	<0.3	<0.3	<0.3
	Mo	Nb	Re	V	Fe	Ni	Co	Ti	Cr	Cu	Rb	Zr
Mo	-	<1	<0.3	<0.1	<0.1	<0.03	<0.03	<0.03	<0.3	<0.03	<0.03	<0.1
W	<1	-	<0.1	<0.1	<0.3	<0.1	<0.03	<0.06	<0.3	<0.03	<0.05	<0.1

Table 1. Content of impurities in the pure molybdenum and tungsten.

4. Growing bicrystals of refractory metals

4.1. Some features of growing bicrystals

Metals and their alloys in the polycrystalline state represent a set of randomly oriented crystallites, or grains, which separated by high-angle boundaries. Properties of polycrystalline materials that are widely used conventionally in materials science and technology largely depend on the size and crystallographic orientation of the constituent grains and, consequently, on the properties of boundaries between the grains. Therefore it is not accidental that the interfacial properties of a type “solid – solid” attracted the most attention of specialists for many years. In recent years a number of theoretical and experimental studies of the interface boundary structure, the energetic and regularities of the grain boundary diffusion and high-temperature creep, the segregation of impurities and structural defects at the interface, as well as processes of heterogeneous nucleation at the interface during phase transitions, is significantly increased [29]. For an experimental investigation of the above phenomena, it is desirable to have samples with well known or readily determinable geometrical relationships between crystallites. From this point of view, of course, the interfaces in bicrystals with known crystallographic parameters are the most convenient and preferable objects. Growing methods of metal bicrystals can be divided into two main groups. The first one includes methods in which oriented bicrystals can be grown from two oriented seeds using standard methods of Chalmers, Czochralski, Bridgman or zone recrystallization. The second group includes methods in which the interphase boundary is obtained by sintering together two plates of oriented single crystals. It should be noted that both groups of methods allow receiving both twist and tilt boundaries, as well as mixed ones. Consider the specific advantages and disadvantages of both

groups. There is a lot of information on getting oriented bicrystals of various metals and alloys by sintering or diffusion welding [30-48]. Using this method to obtain bicrystals usually leads to the fact that boundaries contain a substantial amount of pores and oxide inclusions. Upgraded versions of the method are used to produce bicrystals of copper, silver, nickel, copper-indium and copper-arsenic alloys. In this case, the boundary turns out fairly flat, and does not contain inclusions of the second phase; although sometimes on the boundary an emergence of a small stray of grains of arbitrary crystallographic orientations have been found. Unfortunately, this is not the only downside: sophisticated UHV equipment is necessary for sintering, and the sintering processes last for 10÷20 hours. Furthermore, disks prepared for sintering should be flat and have a surface roughness of not more than 0.1÷0.3 micron, which could be achieved by using diamond polishing pastes. It is clear that before sintering the electropolished deformed surface layer should be removed, otherwise recrystallization becomes inevitable and qualitative boundaries cannot be obtained. Bicrystals of low-melting-points metals can be grown using the method from other group. The essence is that bicrystals can be grown from the melt with the help of two correctly oriented seeds causes no problems at all. Somewhat more complicated is the situation in this way to grow bicrystals of refractory metals such as molybdenum, tungsten, niobium, tantalum, vanadium, *etc.* There is information on growing niobium bicrystals by arc zone melting method [40]. However, this technique does not permit to obtain the required stability of the molten zone and the symmetry of the temperature gradients in the melt and in the solid phase. This leads both to an increased density of dislocations and low quality of the grown bicrystals. The original method of growing bicrystals of niobium by electron-beam zone melting is described in [38]. The essence of this method consists in the following. The single crystalline seed of a cylindrical shape partially cut along a plane of symmetry parallel to the growth axis [110]. Next by moving apart the halves of the original single-crystal seed typed at the desired misorientation angle of the boundary of the bicrystal to grow. Then the bicrystal can be grown simultaneously from both halves of the seed. Thus, the niobium bicrystals of diameter of 6.3 mm and length of 100 mm are obtained. In our opinion, this technique of growing bicrystals, though captivating by its simplicity, but it is too "capricious", on which, however, suggest the authors themselves. They managed to get good bicrystals in only one case out of four. In our view, the failure of the following causes: a poor quality of the electron gun in heating and a complexity of the adjustment of the Y-shaped seed in the thermal zone. Another method of producing bicrystals of refractory metals is described in [30]. The essence of this simple method is as follows: on single-crystal rods the molten zone is created. Then after rotation of the base bar to the desired angle the zone is "frozen". For all its simplicity and attractiveness of this technique it is also not free from shortcomings. First, a small size of a boundary: no more than a diameter of the rod; secondly, the boundary is wavy, as it turns out not as a result of the joint growth of two neighboring grains, but as a result of the "collapse" of moving towards each other two crystallization fronts whose profile in the process of EBFZM is substantially non-planar. In our opinion, the most suitable melting technique for obtaining bicrystals of refractory metals with *bcc* lattice, which do not undergo phase transitions in the solid state, is only EBFZM. This technique allows obtaining a necessary stability of the molten zone and the axial temperature gradient, as well as the required symmetry of the radial temperature gradients. The latter

condition is largely ensures a stability of the growth process of bicrystalline boundaries when growing simultaneously from two seeds oriented in a predetermined manner [36,39]. Stability of the growth of the grain boundary in bicrystals simultaneously from two seed crystals oriented in the predetermined manner, largely due to the symmetry and uniformity of the temperature field. Based on structural features of EBFZM set-up, we would like to note some highlights that should be considered when growing bicrystals of pure refractory metals: (1) the stability and radial uniformity of the power supplied by the electron gun; (2) the co-axiality of the growing bicrystal and electron gun (coincidence of thermal and geometric axes or centers in the liquid zone); (3) the uniformity of the heat removal from the growing bicrystal through the elements of the seed and bicrystal. An important advantage of this method is the possibility of growing bicrystals of up to 150÷200 mm long and up to 15÷25 mm in diameter, suitable for investigating properties of the bicrystalline boundaries both parallel and perpendicular to the growth axis in a large number of reproducible samples. Experiments are carried out on growing bicrystals without rotation, but it turned out that this may affect even minor violations of the local temperature profile in the liquid zone, resulting in one of the growing crystals in the bicrystal can die out. For the manufacture of seeds of 10÷25 mm in diameter and 15÷20 mm in length, consisting of two halves with different single-crystal orientations, the cylindrical single crystals of certain crystallographic directions are used. A deviation from the certain crystallographic direction does not exceed $1\div 2^\circ$. At first, to prepare the parts for the seeds the initial single crystal should be cut by the electroerosion into cylinders of 20 mm long (Figure 2). The cylinders are cut by the diametrical plane to segments for the purpose of obtaining the desired misorientation angle.

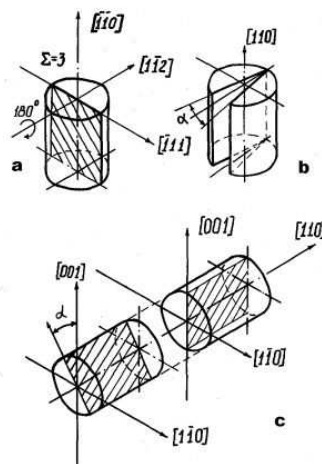


Figure 2. Schemes of preparation of bicrystalline seeds.

The segments of the bicrystalline seed are chemically etched in a mixture of hydrofluoric and nitric acids. Bicrystalline seeds are produced by combining the single-crystalline segments (e.g., 1a+2b or 1b+2a) prepared by the method described above. Another method of preparing the seeds is that one of the segments further cut at an angle equal to the misorientation angle of the bicrystal to grow. This method proved to be a little bit easier, because it does not require

additional operations of the orientation of single crystals. In cases where, besides the misorientation angle, the defined crystallographic parameters should also have the bedding plane of the grain boundary, the plane is defined with respect to which the boundary should be symmetrical. Then a cut is made along a plane that is separated from it by an angle equal to half of the misorientation angle of the bicrystal to grow. The resulting combined two single-crystalline segments after rotation of one of them in the cutting plane by 180° around the axis perpendicular to this plane. Later the plane of the contact between two segments of the bicrystalline seed should be the grain boundary of the growing bicrystal. In the process of the zone growing the grain boundary remains strictly specified and parallel to the axis of the bicrystal and to the axes of both single-crystalline halves of the seed. Our experience has shown that these procedures of preparing bicrystalline seeds are the most important and sufficient for the reproducible growth of bicrystals with any misorientation angle. The method allows growing bicrystals of niobium and molybdenum with the misorientation angles from 5 to 55° . Bicrystals are of 30 mm in diameter and of 100 - 150 mm long (Figure 3). A correct preparation of bicrystalline seeds and a compliance of the optimal temperature distribution allow avoiding pinching one grain by another. The visual and metallographic examinations of bicrystalline samples show that the grain boundaries are macroscopically flat over large areas and do not contain "parasitic" grains or the second phase inclusions. Transverse sections of niobium bicrystals are examined by the optical and scanning electron microscopes, after the mechanical and chemical polishing treatment of the samples in the heated until $50\pm 70^\circ\text{C}$ solution of a mixture of hydrofluoric and nitric acids. Then, the grain boundaries are detected by etching in the same solution at 20°C .

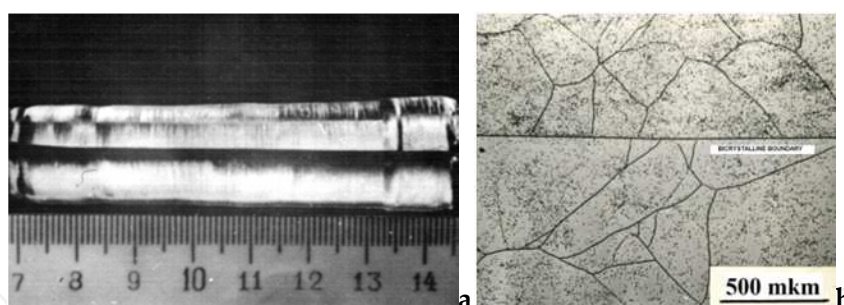


Figure 3. Mo bicrystal of 16 mm in dia (a) and bicrystalline boundary on cross-section (b).

4.2. Studies of strength of high-angle boundaries in molybdenum bicrystals

Tendency of undoped refractory metals of Group 6 (molybdenum, tungsten) to intergranular embrittlement do not only create difficulties in processing, but also significantly reduce the scope of their practical use [32]. Because of complexity of grain boundaries in polycrystalline samples, containing a large and, to some extent, uncontrollable set of grains, studies are carried out on specially prepared bicrystals with well-known crystallographic parameters, because they are the most convenient model objects for the grain boundaries studies. In [30,32,36,49], the dependence of the strength of grain boundaries in molybdenum bicrystals is revealed on

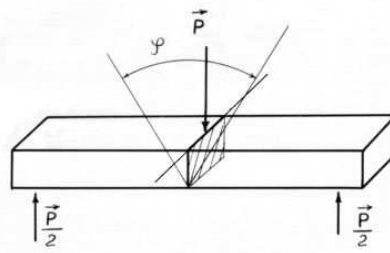


Figure 4. points bend test of bicrystals.

the type of boundaries and the misorientation angle between the grains. By the 3-points bend test (Figure 4) it is established that the high-angle boundaries (over $7\div 10^\circ$) less strong in comparison to low-angle boundaries, and that the higher strength the closer to the boundary planes (100) or (110). It is proved that the twist boundaries in the molybdenum bicrystals are more brittle compared to the tilt ones [41,42]. True, in both types of boundaries (twist and tilt) the possible influence of the bedding plane of the grain boundaries is not taken into account. It should be noted that in the polycrystalline ingots of molybdenum are usually found all types of boundaries and the misorientation angles in different sections of the ingots vary widely. The main reason for the different behavior of the high- and low-angle grain boundaries is the nature of the interaction of these boundaries with impurity atoms. Low-angle boundaries with misorientation angles up to $7\div 10^\circ$, as a rule, consist of lattice dislocations. In the boundaries of high-angle (over $10\div 15^\circ$) the distance between dislocations is so small that their nuclei combine, causing to have different atomic structures. Apparently, impurity atoms by a reaction with the low-angle boundaries are located on their constituent dislocations, whereby the low-angle boundaries occur at areas with a reduced content of impurities. At the high-angle boundaries the impurities segregate more evenly along the boundary, strongly weakening a grip of grains. Therefore, there is an increased susceptibility to intergranular embrittlement. The embrittlement of cast or recrystallized molybdenum largely depends on the interstitial impurities (carbon, oxygen, nitrogen), which, due to the low solubility in the crystal lattice, are allocated along the grain boundaries [41-46]. It was qualitatively shown that at the carbon content of less than $10^{-3}\%$ the strength of bicrystalline boundaries depends on their structure, and above this content - the strength of the bicrystalline boundaries is the same and does not depend on the carbon content. However, it remains unclear why there is the "critical" content, the more that the solubility of carbon and oxygen in molybdenum is by several orders of magnitude lower. Also unclear is the question, what is the relationship between the total content of interstitial impurities in molybdenum and the content of second phase (carbides, oxides) at the grain boundaries. Using the molybdenum bicrystals in studies of grain boundaries usually encounter with serious difficulties in getting bicrystals of given crystallographic parameters, as well in preparing a sufficiently large number of reproducible bicrystalline samples from the same bicrystal.

Apparently, one of the essential crystallographic parameters of the samples is the bedding plane of the grain boundaries, which are still obtained by chance, since the known methods do not allow to grow the molybdenum bicrystals with any desired plane boundary. In the

bicrystalline twist boundaries the axis of twist uniquely determines the plane of the grain boundary. The widest range of the bedding planes of the grain boundaries can be obtained at bicrystals with the tilt boundaries when at one axis in the case of the symmetrical boundaries can exist two bedding planes and in the case of asymmetric boundaries - of any number. In [36,46], the strength of the bicrystalline twist and tilt boundaries in molybdenum bicrystals is studied depending on the misorientation angle between two grains and on the bedding plane of the grain boundary (*i.e.*, the boundaries with a different number of coincident nodes Σ). In [46], the molybdenum bicrystals are grown by the method, the main feature of which is the existence of the optimal temperature distribution in the liquid zone. The samples with twist boundaries are prepared as described in [47,48], but for the growth the better electron gun is used, which allows to create the very narrow liquid zone on the sample and, consequently, more even grain boundaries. In the grown bicrystals the symmetric tilt boundary [100] lies along the plane (120), and the twist boundary - along (100). The bicrystals with the tilt boundaries [100] have misorientation angles and bedding plane other than special boundaries ($\sigma = 36.5^\circ$) with a number of matching nodes $\Sigma = 5$. The bicrystals with the twist boundaries also differ by the misorientation angle of the special twist boundary ($\sigma = 36.5^\circ$) with $\Sigma = 5$. Also, the bicrystals with the tilt boundaries [110] are grown, which are intended for similar studies. In particular, bicrystals are prepared with tilt twin boundaries [110] and the misorientation angle of 70° between the grains and the bedding plane of the boundaries (112) and (111); for comparison it is grown the bicrystal with the misorientation angle of 64° and the plane of the grain boundary, deviated from the (111) plane for 3° . The initial single-crystalline rods, from which the bicrystals are then grown, are prepared in two ways. First, the molybdenum bicrystals (Mo-I) are of a standard purity (*see* Table 2). Secondly, for comparison, the molybdenum bicrystals (Mo-II) of highly-pure molybdenum are grown.

Samples	Impurity content, $\times 10^{-3}\%$					Metallic impurities	Residual resistivity ratio (RRR) $R_{273K}/R_{4,2K}$
	O	C	N	H	W		
I	<0.1	<1	<0.4	<0.1	<3	<1	1500
II	<0.1	<0.01	<0.02	<0.1	<0.3	<0.1	30000

Table 2. Impurity contents and residual resistivity of molybdenum (two levels of purity).

Bicrystalline samples are tested for strength by the three-point bend device (the rate of deformation $0.01-0.1 \text{ mm}\cdot\text{min}^{-1}$). The distance between supports is 9 mm, the radius of supports and the knife - 1 mm. For testing of each bicrystal, 3-5 bars of the size $1,5 \times 2 \times 16 \text{ mm}$ are prepared. The bending axis in bars lies in the plane of the grain boundary and is perpendicular to the common axis of the bicrystal. Tests are conducted at room temperature, and then the fracture stress is calculated by loading curves. The yield criterion is the stress at which plastic deformation is of 0.2%. The dependence of the fracture stress on the misorientation angle of the special (36.5°) tilt and twist [100] boundaries is shown in Figure 5. Topography of fracture surfaces is examined in the scanning electron microscope JSM-T35 at the accelerating voltage of 25-35 kV. Auger spectra of the surfaces of fractured grain boundaries are recorded on the

Auger spectrometer PHI-551 with the base residual pressure in the chamber, not exceeding 1×10^{-7} Pa. "Fresh" surfaces of the grain boundary fracture are obtained in the pre-chamber of the Auger spectrometer at vacuum of 1×10^{-5} Pa. The spectrum recording time - no more than 1 min, the focal spot diameter - 10^{-5} m. Grain boundaries are revealed by etching in the mixture of nitric and sulfuric acids. For the X-ray diffraction study of the grain boundaries, the bicrystalline samples are mechanically polished and electropolished in a concentrated sulfuric acid. Laue patterns are obtained from individual grains with an accuracy of $1 \pm 2^\circ$. The tests have shown that almost all bicrystals have the brittle fracture, although on some of them plots of plastic deformation before fracture are observed (Table 3). The fracture of specimens under the applied load passes strictly along the grain boundary. The study by the optical microscope reveals that all samples have the flat boundary parallel to the axis of the bicrystal. Without plastic deformation, the fracture stress perpendicular to the grain boundary is calculated from the load to fracture, considering the sample as the elastic bar.

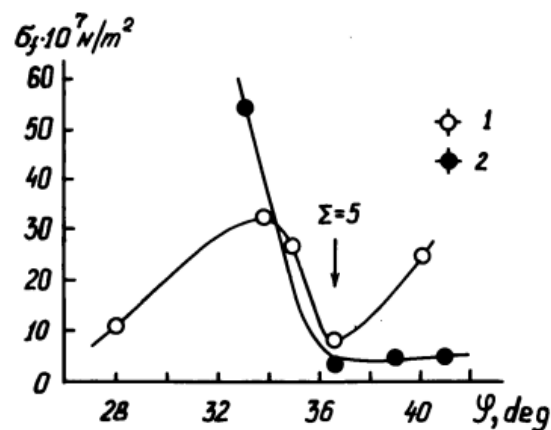


Figure 5. Fracture stress vs. misorientation angle.

Strength does not exceed the fracture stress of the boundaries on the cleavage plane (100) and depends both on the misorientation angle between the grains and on the bedding plane of the grain boundary at the same misorientation angle between grains. The significant stress of the fracture equal 30×10^7 N m⁻² is observed on the sample Nr 13 with the boundary of a general type; the fracture takes place with appreciable plastic deformation (up to 7%). The fracture stress equal 25×10^7 N m⁻² is obtained on the sample Nr 11 with the twin tilt boundary lying in the incoherent twinning plane (112). This bicrystal has an elongation approximately 1%. The stress fracture of the sample Nr 12 with the twin boundary and the bedding plane along the coherent twin plane (111) is 11×10^7 N m⁻². On the sample Nr 10 with the misorientation angle of 64° the fracture stress is equal 15×10^7 N m⁻². The molybdenum bicrystals with the special tilt and twist [100] grain boundaries are fractured at low loads and often uncontrollable, although the boundaries other than special, it turns out, tend to be of the much higher strength. The strength of the tilt boundaries [100] with the misorientation angle of 33° reach relatively high values - 55×10^7 N m⁻², although at other angles the strength is low (below 10×10^7 N m⁻²). The twist boundaries [100] at the misorientation angles of $34 \pm 35^\circ$ and 40° are quite strong -

$(25\pm 30)\times 10^7 \text{ N m}^{-2}$, but at 28° the strength decreases to $10\times 10^7 \text{ N m}^{-2}$. It is seen in Figure 5 that in the special boundary minimum of the strength is observed for twist and tilt boundaries in the region adjacent to the angle of 36.5° . To test the effect of the bedding plane of the grain boundary on its strength the bicrystal is grown. It contains the misorientation angle 33° and the bedding plane deviated by 45° from the plane of the boundary in the bicrystals with the greatest strength, equal $55\times 10^7 \text{ N m}^{-2}$. The tests have shown that the strength of such boundary is almost five times lower. According to [45], the orientation dependence of the strength of the grain boundaries is of the monotonous character and the strength of the tilt and twist boundaries in the range of angles from 20 to 45° , as a rule, does not exceed $(8\pm 10)\times 10^7 \text{ N m}^{-2}$. The slight deviation from the monotony is found for the twin tilt boundaries [100]. In [44], extremes are found on the orientation dependence of the tilt boundaries [110] with the misorientation angles of approximately 10° and 55° , but absolute values of the fracture stress for the boundaries of both types are too high – up to $(100\pm 150)\times 10^7 \text{ N m}^{-2}$, *i.e.*, even exceed the tensile strength of the molybdenum single crystals and, apparently, is incorrect. Kinks on the twist boundaries are shown in Figure 6. It is clearly visible chains of the second phase precipitates (presumably, carbides) at the terraced kinks and precipitates like needles at right angles to each other.

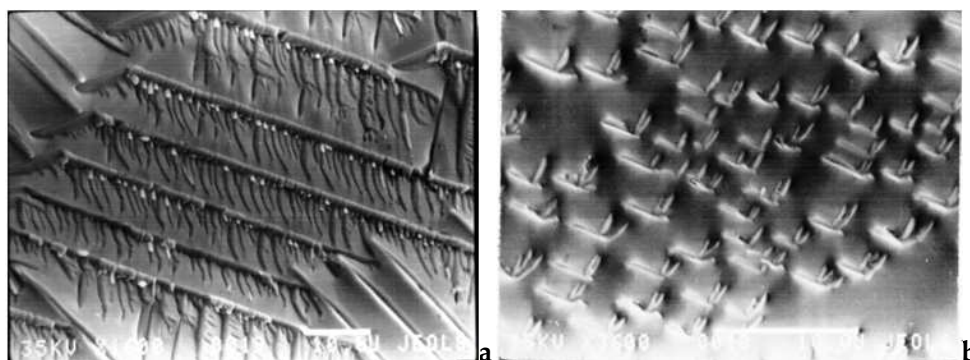


Figure 6. Fractography of the fracture surface of the twist [100] grain boundary (a) and of the tilt twin boundary [110] (b).

It should be noted that on the fractures of the twist bicrystalline boundaries of Mo-II the significantly smaller amount of the second phase is present, in comparison to samples from Mo-I. The molybdenum bicrystals with special twist boundaries, however, are fractured with the uncontrolled stress, although the precipitates at the fractured boundaries are virtually absent. The small precipitates in a form of thin films on fractured surfaces of the special tilt boundaries are observed; however, they disappear when exposed to the electron beam. Analysis of Auger spectra from different areas of the fracture surface of tilt boundaries [110] has shown that the intensity of Auger peaks of carbon, oxygen and nitrogen is varied. Near the outer surface there is the extended zone of a width $0.1\pm 0.2 \text{ mm}$, in which the oxygen content is 20% higher in comparison with central areas. On peripheral areas there is also the high nitrogen content; however, at central areas at the grain boundary the intensity of Auger lines is close to zero. The intensity of Auger lines of carbon, conversely, is increased from the periphery to the center. These data, of course, are qualitative in nature, as in the pre-chamber

Sample	Boundary	Misorientation angle, angular degree	Bedding plane of boundary	Σ	$\sigma_f \times 10^7,$ H m ⁻²
1	Tilt [110]	17	(551)	-	14
2	Tilt [110]	20	(119)	33	10
3	Tilt [110]	26	(331)	19	17.5
4*	Tilt [110]	26	(331)	19	3.5
5	Tilt [110]	39	(221)	9	12.5
6*	Tilt [110]	39	(114)	9	14
7	Tilt [110]	39	(114)	9	8
8	Tilt [110]	50	(113)	11	9
9*	Tilt [110]	50	(113)	11	3.7
10	Tilt [110]	64	(111) dev.3°	-	15
11	Tilt [110]	70	(112)	3	25
12	Tilt [110]	70	(111)	3	11
13	Tilt [110]	General type	-	-	30
14	Tilt [100]	33	-	-	55
15	Tilt [100]	36.5	(120)	5	3
16	Tilt [100]	39	-	-	9
17	Tilt [100]	41	-	-	8
18	Twist [100]	28	(100)	-	11
19	Twist [100]	35	(100)	-	31
20	Twist [100]	35	(100)	-	27
21	Twist [100]	36.5	(100)	5	8
22	Twist [100]	40	(100)	-	25

*bicrystals grown from Mo-II.

Table 3. Crystallographic and strength characteristics of samples with the tilt and twist boundaries [110] and [100].

of the Auger spectrometer the residual pressure is such that the number of atoms colliding with the surface for one second corresponds to one atomic layer, while the process of transferring the sample in the chamber of the Auger spectrometer takes about 10 minutes. The Auger spectrum of the fracture surface of the sample Nr 7 shows that it contains lines, except the molybdenum line, of carbon (272 eV) and oxygen (503 eV). The low intensity line (380 eV) is, apparently, due to nitrogen. A peak of oxygen should be partially attributed to the adsorption of oxygen from the residual gas in the pre-chamber. A form of the Auger carbon line reveals that it is partially caused by adsorbed hydrocarbons, and partially - by a presence in the analysis zone of molybdenum carbide, as evidenced by the low-energy characteristic of the comb structure of lines. It is unlikely that in the presence of the significant amount of dissociated oxygen the surface carbide formed immediately after destruction of the sample along the bicrystalline boundary. Most likely, the Auger spectrum has elicited the three-dimensional carbide precipitates that already exist on the grain boundary. After the ion etching of the fracture surface at the grain boundary the contents of elements in the area of the analysis have

been varied somewhat. The intensities of Auger lines during the etching of the sample Nr 7 show that at transition to deeper layers carbon and oxygen decrease as compared with the "fresh" fracture surface.

The shape of the Auger line of carbon during etching also varies considerably and becomes fully "carbide-like". Due to the lower sputter coefficient of carbon compared with the sputter coefficient of molybdenum, the carbon accumulation can occur near the surface. The absolute value of the ratio C/Mo determined from the Auger spectra after the prolonged etching is substantially overstated. To correct the carbon content profile in view of this accumulation is not yet possible; however, given in Table 4, the values of C/Mo permit make a comparison between the samples by the volume content of carbon, so long as at the prolonged etching the enrichment of carbon should be proportional to the volume content of carbon. Oxygen distribution is the same for all bicrystalline samples, although in the course of ion etching the intensity of the Auger line of oxygen falls. The region, rich of oxygen, is no more than 80 Å. The character of distribution with the depth is different for all the samples, but the intensity of the Auger line falls with the depth. On some specimens the marked intensity of the Auger lines persists to a depth of 800÷6000 Å. The maximum intensity of the Auger line of molybdenum is in the range 20÷50 Å. It is because the early etching removes contaminated layers in which the content of molybdenum is relatively lower than in the matrix. In the course of etching the analyzed surface roughness caused by uneven etching of its various portions is enhanced, which leads to additional scattering of the Auger electrons. Because of low solubility of interstitial impurities in molybdenum at cooling rates typical for growing molybdenum bicrystals they are allocated as the second phase. While it is not possible to correctly assess the degree of enrichment of the grain boundaries with the interstitial impurities or precipitates. It can only be based on comparison of the relative content of interstitials on the tilt and twist boundaries. At the "fresh" fracture surface and at the depth of up to 1000 Å from the surface, it is possible to argue that the degrees of "contamination" of the boundaries of both types are identical. Secondly, it can be concluded that most of the carbon on the fracture surface is bound to carbide precipitates.

Grain boundary	Analyzed layer depth, Å	Ratio of analyzed elements			
		C _{tot} /Mo	C _{carb} /Mo	N/Mo	O/Mo
Tilt	0	1.60	0.55	0.01	0.45
Tilt	1000	-	1.40	0	0.08
Twist	0	1.26	0.56	0.13	0.36
Twist	1000	-	1.38	0	0.12

Table 4. Ratio of chemical elements on the surface of the grain boundaries and at the depth of up to 1000 Å from the surface of the tilt and twist grain boundaries [100].

Of particular interest is comparison of bicrystals with the different initial purity. Although the content of interstitials in Mo-II is much lower even in comparison with pure Mo-I, the boundary strength of the tilt bicrystals, grown from Mo-II, differ a little from the strength of the samples of Mo-I. This is all the more surprising that, according to the Auger analysis at

grain boundaries of samples grown from Mo-I, as the carbon content on the fracture surface, and in the depth of grains is substantially higher. The oxygen content is the same at boundaries of all samples. In [43,45], argued that the fracture stress of twist boundaries is inversely to the oxygen content on boundaries, and the role of carbon was reduced mainly to suppress this effect. Experimental results obtained so far are not enough to talk about any influence of oxygen on the strength of grain boundaries. The boundary strength of pure molybdenum, which conducted the present study on, is primarily dependent on high misorientation angles of boundaries, and change of the total content of interstitials in the investigated content range does not lead to any noticeable change in strength.

4.3. Studies of fine structure of low-angle boundaries in tungsten bicrystals

In *bcc* metals is most likely the presence of dislocations with Burgers vectors of $a/2[111]$ and $a[100]$, where, a is the period of a cubic lattice [23,41,48]. However, there is no information about the presence of dislocations with Burgers vector $a[110]$ in the *bcc* metal crystals. Low-angle boundaries and the characteristic dislocation substructure, particularly of tungsten, are formed from these dislocations arising during the crystal growth (probably due to high thermal stresses). There is tendency to form low-angle boundaries of tilt or twist at the relatively low dislocation density in the crystal ($\sim 10^5 \div 10^6 \text{ cm}^{-2}$) [48]. Such boundaries may consist of one (for tilt boundaries - symmetric), two, three or more families of dislocations. The fine structure of such boundaries has been comprehensively investigated in [22,23] on single crystals of tungsten and molybdenum exposed to the high-temperature creep. An average size of subgrains in such crystals is several microns. Low angle boundaries have the misorientation angle in the area $2 \div 4^\circ$, but consisted mainly of dislocations introduced in the crystal by means of plastic deformation instead of so-called dislocation growth. It should be noted that the dislocation model of low-angle boundaries is well established. Systems of dislocations forming low-angle boundaries are in the metal lattice and tend to have the lowest energy in crystallographic planes being located close to crystallographic planes of low indices. In particular, for the *bcc* lattice symmetrical tilt boundaries consisting of parallel edge dislocations, are most likely in planes $\{111\}$ and $\{100\}$, asymmetric tilt boundaries - in planes of $\{hko\}$, and net twist boundaries - in planes of $\{110\}$. Thus, if to the system of dislocations, created in the flat layer of the low-angle misorientation, provide the opportunity to move (by glide and climb of), the system of low-angle boundaries should strive for the finite number of planar nets. All of the above indicates that the triple junctions of low-angle boundaries do not necessarily have to be of 120-degree. In some cases, low-angle boundaries are observed on facets on the microscale, what also appear crystallographic structural features of low-angle boundaries. It is known that the crystal grown from the seed inherits its substructure. The seed already contains stable low-angle boundaries which germinate in the growing crystal. If the bedding plane of boundaries is parallel to the crystal growth axis, such low-angle boundaries remain in the crystal and germinate over long distances, for example, in the axis and having the misorientation angle up to $1 \div 2^\circ$. Using the method of stereometric metallography we found that the bedding plane of the sub-boundaries with an accuracy of $1 \div 2^\circ$ corresponds to crystallographic planes of the type $\{100\}$ (Figure 7a). Low-angle boundaries are identified by etching on the plane of the single crystal W(010) with the growth axis $[001]$.

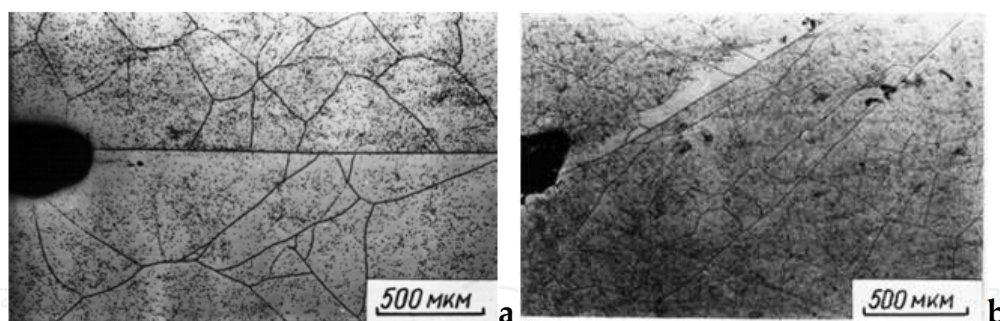


Figure 8. Symmetrical low-angle twist boundary (a), occurs in the $\{110\}$ plane and grows in the crystal with the growth axis $[110]$ and the low-angle tilt boundary (b) created artificially in the $\{110\}$ plane, which tapers off the crystal.

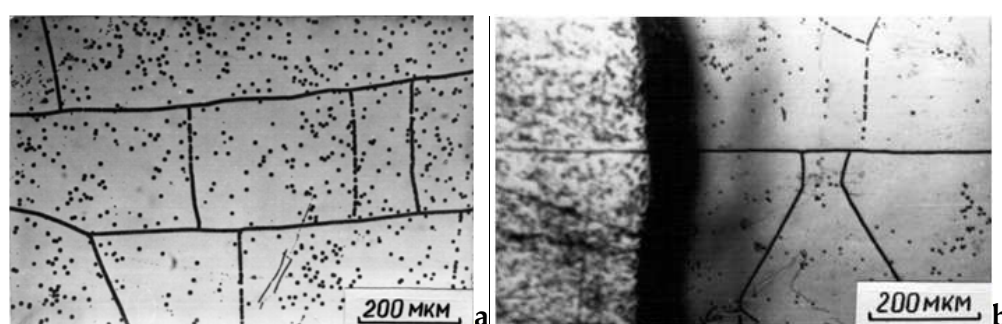


Figure 7. Low-angle boundaries: on (010) plane, growth axis $W[001]$ (a), and on (100) plane along $W[100]$, the stereometric metallography (b).

On Figure 7b metallographic cross-sections presented with a plane parallel to the axis of the crystal growth $[001]$ correspond to the plane (010) and contains the step with a height of about 300 microns, which is greater than the depth of the focus of the microscope objective and the top of the stairs because blurred. However, it is seen that the sub-boundary located in the center is in the $\{100\}$ plane. Earlier, similar results were obtained in [50] by X-ray topography. It would certainly be interesting to investigate the fine structure of such small-angle boundaries, *i.e.*, decipher Burgers vectors of constituent dislocations, but, unfortunately, to prepare suitable electron microscopic samples is not yet possible. In principle, it is possible to create the low-angle twist or tilt misorientation in any crystallographic plane parallel to the crystal growth axis by the preparation of bicrystals. However, if in this plane cannot be obtained the artificially created misorientation by using the known complete lattice of dislocations, such low-angle boundaries cannot exist and should be quickly tapered off the crystal during the growth. Several tungsten bicrystals containing low-angle tilt or twist boundaries are grown. The characteristics of these boundaries and results of their growth are given in Table 5. For example, the pure twist boundary in the plane $\{110\}$ is possible and it grows into the crystal, but the symmetric tilt boundary – no, and, naturally, it tapers off in the growing process, which shown in Figure 8.

The dislocation structure of low-angle boundaries in the tungsten single crystal is presented in electron micrographs (Figure 9a). On Figure 9b, the corresponding electron diffraction

pattern of the area containing low-angle boundaries is shown. The foil plane corresponds approximately to the $\{111\}$ plane. Having completed a flat grid of a reciprocal lattice (Figure 9c), it can be shown that the trace of the plane crossing the low-angle boundary and the foil plane is the direction $\vec{l} = [4\bar{5}1]$. Unfortunately, the sample was too thick and the determination of Burgers vector of dislocations forming the sub-boundary, in contrast attenuation condition $\vec{g}\vec{b} = 0$, is failed.

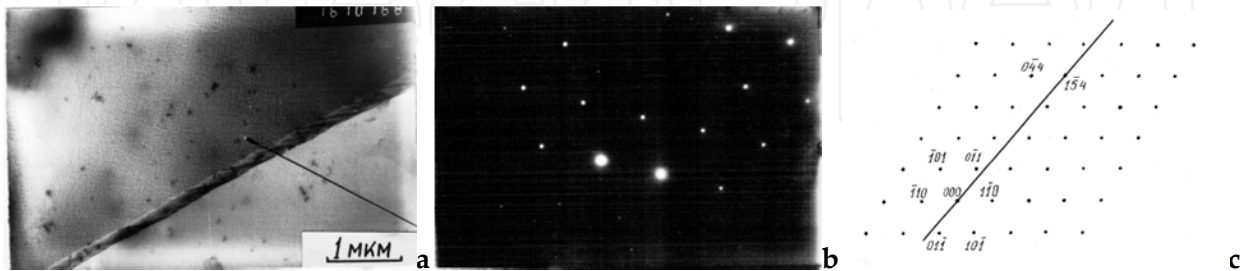


Figure 9. Electron micrograph (a), electron diffraction pattern (b) & flat grid of a reciprocal lattice reconstructed (c) of the small-angle twist boundary in W bicrystal.

Sample	Growth axis	Bedding plane of boundary	Boundary type	Results of the growth
1	[100]	{110}	Tilt	Taper off
2	[100]	{110}	Twist	Grows in crystal
3	[100]	{100}	Tilt	Grows in crystal
4	[100]	{100}	Twist	Grows in crystal
5	[110]	{110}	Tilt	Taper off
6	[110]	{110}	Twist	Grows in crystal
7	[110]	{100}	Tilt	Grows in crystal
8	[110]	{100}	Twist	Taper off
9	[110]	{111}	Tilt	Grows in crystal
10	[110]	{111}	Twist	Grows in crystal

Misorientation angle of low-angle boundaries always in range from 1° to 3°

Table 5. Crystallographic parameters of the tungsten bicrystals with the low-angle boundaries.

However, the available information, in particular about the angle $\gamma = L(\vec{\vartheta}, \vec{l})$, leads to the conclusion that the presented sub-boundary is the twist low-angle boundary and consists of two families of screw dislocations with Burgers vector $(\vec{b} \parallel \vec{\vartheta}) \vec{b} = a/2[111]$. The low-angle

boundary plane is $n = (134)$, and the corresponding Burgers vectors of screw dislocations are $\vec{b}_1 = a/2 [\bar{1}\bar{1}1]$ and $\vec{b}_2 = a/2 [\bar{1}11]$. The structure of the boundary is different on different sites. It is possible to find a site of the low-angle boundary, in which dislocations of one of the families are placed non-equidistantly, but at intervals 3-4-3-4. Thus, the specific dislocation structure of low-angle boundaries formed by growth dislocations can be very difficult to reveal.

4.4. Studies of molybdenum bicrystals by low-energy ion scattering

Bicrystals, consisting of two differently oriented grains of high structural quality and purity, and grain boundary plane are the excellent models for experimental studies of various physical properties of both the surface and the grain boundary [37,51-55]. Here, the dignity of bicrystals in the studies of surface and bulk processes is shown for segregation, atomic reconstruction and self-diffusion on different crystallographic surfaces. Specifically targeted surfaces of the molybdenum bicrystals presented preselected surfaces of two grains (single crystals) and an interface therebetween. In this case both the grains are grown in exactly the same conditions, and processing of both grain surfaces is carried out in fully identical conditions. The specimens are cut of the massive molybdenum bicrystals normally to their axes, so the bicrystalline boundary is always at the centre of the flat specimens. The specimens are studied by low-energy ion scattering (LEIS). This method has a very high surface sensitivity and allows studying selectively processes taking place in the uppermost atomic layer. The LEIS signal intensity is directly proportional to the density of atoms on the surface and, therefore, must be different for differently oriented surfaces. Until recently, the LEIS technique is used for detailed studies of the surface structure of single crystals and various adsorbents on it by the angular dependence of the LEIS signal. However, the dependence of the scattering intensity of the ions from the atomic density is not obvious, experimental studies of this relationship are still not enough. Unfortunately, almost no studies that compare the LEIS signal intensities for differently oriented surfaces of the same object. The only study was done on silicon many years before where LEIS signals from the Si (111), Si (110) and Si (100) are compared. However, the ion doses used at that early time were so high that they cause severe destruction of the surface. Most likely, the correlation is discovered by accident. Now, we are able to identify and compare atomic densities on the surfaces of different low indexes single crystals and bicrystals of molybdenum and tungsten.

A clearer understanding of the crystallographic dependence of the signals is very important for the quantitative analysis by LEIS. For example, in the case of single-crystalline surfaces and adsorbents, this method allows getting detailed information about the atomic structure. The advantage of LEIS - an opportunity to get a statistically average result, since the scanning ion beam has a permanent, fixed diameter (from about 10 microns to about 1 mm). In the case of non-homogeneous samples scanning is possible perhaps even on an area of 1 cm². Problems arising in the study of the crystallographic dependence of the LEIS signal, may partly explain the lack of experimental evidence; however, this relationship can only be measured on clean and well-oriented surfaces. Moreover, for comparison of two different crystallographic planes it is indispensable the preparation of the specimens in absolutely identical conditions. These problems can be successfully solved by using bicrystals. In conducting the present study were

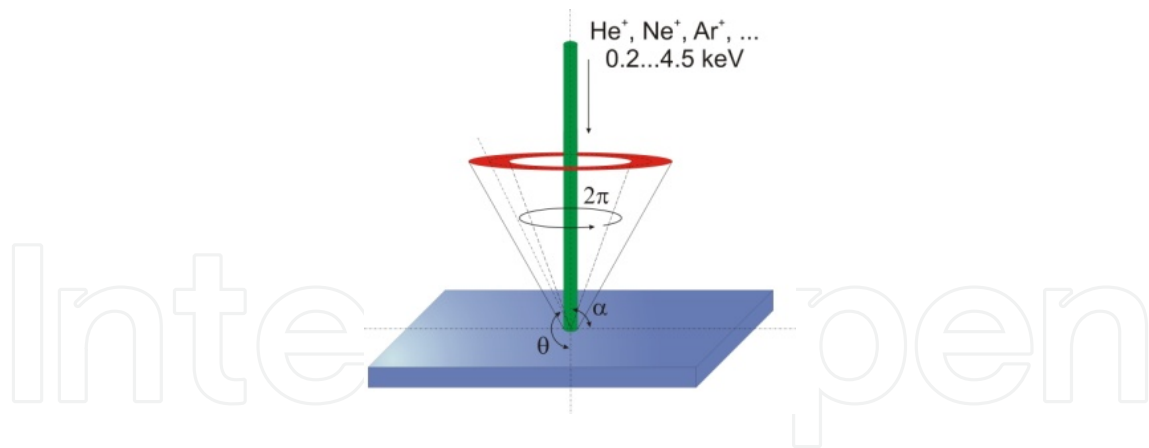


Figure 10. Scheme of the LEIS experiment.

prepared surfaces of molybdenum bicrystals Mo(110) and Mo(100). These planes have been chosen due to differences in the density of atoms on the surface. Thus, Mo(110) is a close-packed surface with the higher density of atoms in *bcc* structure, and Mo(100) - an "open" surface with the lower density of atoms. Both surface planes are the perfect single crystals with crystallographic orientations of Mo[110] and Mo[100]. The bicrystalline boundary separating two single crystals in the center of the sample, held on {100} plane, is macroscopically smooth over the entire sample and does not contain "parasitic" inclusions of other phases. For the LEIS study, the "Mini-Mobis" with a base pressure of 2×10^{-10} mbar is used. The unit is equipped with measuring devices for LEIS, Auger electron spectroscopy (AES) and low-energy electron diffraction (LEED). When measuring by LEIS, the monoenergetic beams of Ne^+ ions and $^4\text{He}^+$ ions with energy of 3 keV are used. The beams bombard the sample in direction perpendicular to the surface of the sample. The ions, scattered at an angle of 136° , are detected by the analyzer of the "cylindrical mirror" type. This analyzer is used also for Auger measurements. To avoid structural defects on the surface of the sample during the experiment the ion doses do not exceed 10^{14} ion cm^{-2} . The diameter of ion beam is about 400 microns, since for some LEIS intensity measurements in the boundary region between two grains (crystals), the diameter of the beam is too large, so a part of experiments are conducted on a similar LEIS set-up in which could be used the ion beam of the diameter up to 25 micron. It is comparable to the thickness of the grain boundaries in the bicrystals under study. Heating of the samples is carried out *in situ* by means of special cathodes consisting of a heating element and a source of electrons. Between the sample and the cathode an accelerating voltage is applied. As a result, electrons bombard the surface of the sample, causing thereby its rapid heating to temperatures of approximately 2500°C . For the present study there are grown two different molybdenum bicrystals by electron-beam floating zone melting. One bicrystal contains two grains (crystals) Mo[110] separated by a tilt boundary with a misorientation angle of 70° between grains (crystals). Another bicrystal contains grains (crystals) Mo[100] and Mo[110] separated by a 45-degree twist boundary. Both molybdenum bicrystals of 15 mm in dia are cut into the plates of $7.5 \times 7.5 \times 1 \text{ mm}^3$. Thereafter, the plates are subjected to the mechanical and electrolytic polishing, followed by annealing in an oxygen atmosphere. The study of bicrystalline samples by LEIS is carried out after the final cleaning the surface *in situ* by the electron gun with a rapid heating

to 2500°C directly in the measuring chamber. To reduce contamination of the samples in the measuring chamber, near-by elements of chamber are made of the massive high-purity molybdenum. Experiments are performed on atomically clean surfaces that are monitored by LEIS, AES and LEED. The residual contents of carbon and oxygen are below the sensitivity of LEIS (<0.1% of the monolayer using $^4\text{He}^+$ ions with energy of 3 keV). With LEED could be seen a clear picture of the crystallographic planes (110) and (100), corresponding to two grains (crystals) of the molybdenum bicrystals. After long exposure of the specimens in the measuring chamber even in UHV, an intensity of the LEIS signal dropped, apparently due to adsorption of atoms of the residual gases present in the chamber. After repeating short heating, the sample surface becomes clean again. The quadrupole mass-spectrometer, mounted in the measuring chamber, shows that the main impurity in the annealing chamber during the sample annealing - the elements of masses 2 and 28, which correspond to nitrogen and hydrogen (or carbon monoxide), respectively. At the beginning of the experiment the surface of both grains (crystals) Mo(111) and Mo(100) are at the same level of the sample (by height). However, after "vacuum oxy-polishing" of the molybdenum bicrystal, both grains (crystals) are at different levels depending on their crystallography, and the boundary groove appeared after vacuum etching (Figure 11), the slope of the sides of which also depends on the crystallographic orientation of the grains (crystals) constituting the bicrystal.

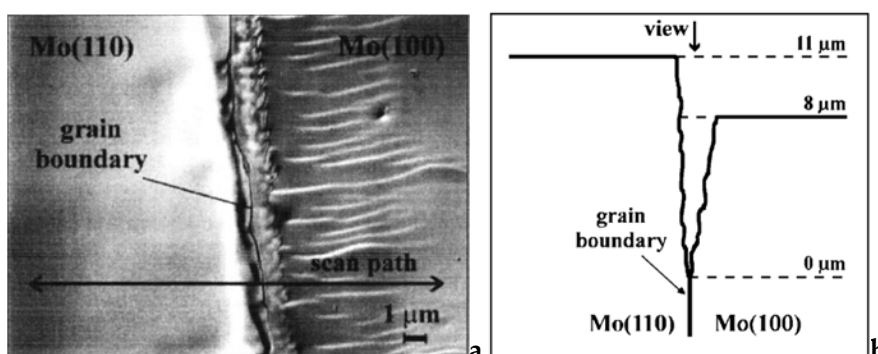


Figure 11. SEM micrograph of a Mo bicrystal, top view (a), and graphic profile (b) of the bicrystal boundary.

Experiments are carried out by scanning the surface of the bicrystal by a narrow beam of Ne^+ ions with the diameter of 25 microns and energy of 3 keV. The measured elastic peak of the molybdenum intensity is a function of the ion beam position on the surface of the bicrystal. The studies of the bicrystal, in which both grains (crystals) are of the similar surface orientation Mo(110) and the tilt boundary, do not reveal any difference in the signal intensity between two grains (crystals). This shows that the crystallographic orientation of the surface plane itself has no effect on the value of the LEIS signal intensity, so the greatest interest is the molybdenum bicrystal with different orientations of the two grains (crystals). Interestingly, the heat treatments result in difference of segregation of carbon at different crystallographic surfaces. After the prolonged anneal of the bicrystalline sample in UHV (1 hour at 1100°C), carbon segregation from the volume on the surface Mo(100) has been detected (Fig. 12a). Naturally, at the initial state the molybdenum bicrystal has the same carbon concentration in both the

grains (crystals). The volume carbon concentration does not depend on the crystallographic orientation of both surfaces of the grains (crystals). In addition, on the surface of the grain Mo(100) the carbon atoms in the initial state are not fixed at all. Carbon occurred as a result of the annealing the surface (100) is then removed by *in situ* annealing in an oxygen atmosphere ($\sim 10^{-6}$ Pa) at about 1500°C. However, after the prolonged anneal at about 1100°C it again appears on the surface Mo(100). In the study of the crystallographic dependence of the LEIS intensity, the signal of molybdenum is normalized to the most densely packed plane (110). It has been established (Figure 12b) that there is a clear dependence of the LEIS signal intensity from the crystallographic orientation of each grain (crystal). The presence of the grain boundary between the different planes is marked by a sharp change of the signal in position 0. The ratio R of the signal from the surface Mo(100) to the signal from the Mo(110) is found to be 0.74 ± 0.02 , which is slightly higher than the ratio of the atomic densities for these crystallographic planes (0.707). As shown in [6,8], for the close-packed crystal surfaces of tungsten and rhodium, contributions to the LEIS signal intensity from the second and third atomic layers are negligible. This means that for these surfaces the signal intensity is proportional to the surface density of atoms at the uppermost atomic layer. Since we found almost exact ratio of the signals from the surfaces of Mo(110) and Mo(100), this suggests that even for an "open" plane (100) the contribution from the second and third layers to the elastic peak is negligible. To study the effect of ion bombardment on the LEIS signal, the Mo(110)/Mo(100) bicrystal is subjected to ion sputtering by the defocused ion Ne^+ beam with energy of 3 keV at room temperature. The ion dose is in the range from 7×10^{15} ion cm^{-2} to 40×10^{15} ion cm^{-2} at a constant ion current 6×10^{-12} ion $\text{cm}^{-2} \text{ s}^{-1}$. After ion bombardment, a repeated measurement is done of the same surfaces of the sample as before sputtering (Figure 12b). The measured scan shows that after ion bombardment there is the significantly decreased signal intensity, especially for the molybdenum surface Mo(110), where the signal is decreased by 25%, whereas for molybdenum surface Mo(100) - only by 10% (see Table 6).

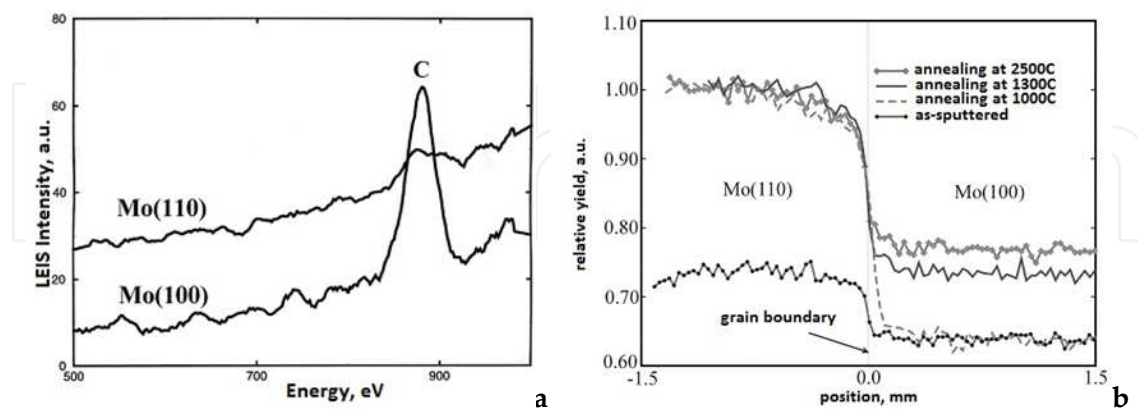


Figure 12. Spectra: C segregation on Mo(110)/(100) faces (a) and recovery of LEIS yield on Mo(110)/(100) faces (b).

Sputtering increases the surface roughness. This effect can be understood if we consider the sputtered atoms from the surface Mo(110). At first glance, in this situation, for the incident ion it is easier to penetrate into the second atomic layer and not to be neutralized in the first atomic

layer. Yet it is unlikely that ions could be reflected in the opposite direction and go back through the top atomic layer, remaining ionized. This situation is indeed confirmed by our experiments, since the ion beam is directed to the sample surface normal and the detector detects only ions scattered at an angle of 136° , so the sputtered atoms of the first atomic layer from the surface Mo(110) leads to decrease in the effective atomic density. However, when a sufficiently large number of atoms will be sputtered, dynamic equilibrium will be established, because accumulation of single vacancies should make the second atomic layer more open. For the Mo(100) surface, which is already quite "open", the possibility of backscattering from the second atomic layer after surface sputtering will be much greater. Thus, it becomes clear why decrease of the LEIS signal intensity after sputtering is more significant for the close-packed Mo(110) surface. Even at high doses of sputtering, the difference between the signal intensities from the different crystallographic surfaces still remains. This is partly due to the conservation of the structure in the bulk crystal, and partly due to the fact that ion etching not only makes the surface amorphized, but also removes a lot of layers. At a dose of 40×10^{15} ion cm^{-2} , almost hundred atomic layers are removed from the surface, which far exceeds the range of thicknesses where Ne^+ ions with energy of 3 keV could make the surface amorphized. Apparently, the result of these processes is dynamic equilibrium.

Treatment	Relative LEIS yield		Atomic density ($\times 10^{15} \text{ cm}^{-2}$)	
	Mo(100)	Mo(110)	Mo(100)	Mo(110)
As sputtered	0.73	0.64	1.02	0.91
700K, 1 min	0.89	0.64	1.25	0.91
1000K, few seconds	0.97	0.64	1.47	0.91
1300K, 3 minutes	0.99	0.73	1.40	1.03
1600K, flash	1.00	0.76	1.41	1.07
2500K, flash	1.00	0.76	1.41	1.07
Ideal lattice, first atoms, normalized to (110)	1.000	0.707	1,41	1.00

Table 6. The relative LEIS yields and atomic densities of the Mo(110) and Mo(100) after various annealing treatments.

After sputtering, the molybdenum bicrystal is annealed at different temperatures and scanned along the surface by the ion beam of Ne^+ with energy 3 keV. In this case, the amplitude of the elastic peak is recorded as a function of the position of the ion beam (Figure 12b). Measurements show that recrystallization of the surface Mo(110) after ion bombardment begins at about 700°C and completed at about 1100°C , and for Mo(100) recrystallization starts at $\sim 1300^\circ\text{C}$. After high temperature annealing ($\sim 2500^\circ\text{C}$) the signals are the same as in the initial undamaged clean surface. Based on this, it is supposed that the different surface structures have different mobility of atoms, and the difference of the signal intensities can be used as a measure that determines the amount of disorder in the surface. The high mobility of atoms in the upper

atomic layer of Mo(110) is supported by the lower surface energy of the molybdenum "close"-packed structure (110) as compared to "open" Mo(100).

5. Growing tube single crystals of refractory metals

5.1. Main features of growing tungsten tubular single crystals

Shaped tungsten single crystals are used as screens of different shapes, inputs, crucibles, shapers and other products. There is considerable interest to profiled tubular shaped single crystals (primarily, of tungsten) in connection with their use in prospective designs of thermionic converters. The production of tubular tungsten single crystals from bulk cylindrical crystals by traditional machining (drilling, broaching) is extremely labor-intensive, low-tech and uneconomical process. Get such tubes pulling from the melt, for example, by Stepanov method, is impossible even for the reason that there are no available materials for the shaper. The only possibility to obtain single-crystalline tungsten tubes by crystallization from the melt is to use for this purpose EBFZM method. Various materials can be successfully applied in industry to create structures, machine parts and devices only if they can be given in the required shape. Such shaping of crystalline materials may be done of the solid material (rolling, forging, shaping by cutting, *etc.*) and liquid phase (casting, welding). The shaping methods are now widely used to obtain polycrystalline products. Recently, in science and technology becoming more widely used are single crystals in the form of plates, tubes, rods of various sizes. In principle, the single-crystalline tube may be cut out from a bulk single crystal by mechanical or electrical discharge machining. However, using such kinds of processing, the single crystal will inevitably contain multiple structural defects that can alter the properties of the crystal in an unpredictable manner. For example, during the electroerosion cut of tungsten single crystals a network of cracks in the sub-surface layer occurs, and the dislocation density increases. Furthermore, such treatments are inefficient; too much of waste material is usually lost. The low economic efficiency and non-technological methods have led to search of alternative methods of getting profiled single crystals. Among them are plastic deformation, epitaxial growth from the gaseous phase, crystallization from a molten solution, crystallization from the melt. Advantages of the latter forming method consist mainly in the higher productivity and better quality (because of both the structure and properties) of the final product. Crystallization from the melt provides the most perfect structure and high purity of single crystals because of the contact-less melting with no contaminating material at the front of crystallization (*e.g.*, Czochralski method). However, due to the low stability of the capillary shaping this method can allow obtaining only products of the simplest form – the rods. Verneuil method, including plasma heating, allows obtaining single crystals of various materials in the form of tubes. It seems that the most suitable method for obtaining the tubular single crystals by crystallization from the melt is Stepanov method. The method consists in a capillary shaping of the column from the melt using a special shaper and its crystallization proceeds outside the container with the melt. Stepanov method has a significant margin of stability and enables the profiled metal and semiconductor crystals of high quality. A float zone method can also be used for crystallization of single crystal tubes from the melt. An

example of using this method to obtain tubes can be found in the monograph by Pfann [8]. In principle, the float zone methods may use any heating source, but the most suitable method to obtain the tungsten tubular single crystals with thin walls is floating zone method with electron-beam heating [60-62]. Until now, by the method of EBFZM from the melt were grown the most perfect and the purest single crystals of tungsten and other refractory metals. Crystals obtained by this method typically have a cylindrical shape. EBFZM method seems to be the most promising for growing shaped single crystals of tungsten and other refractory metals in the form of tubes. Growing tubular crystals of tungsten was done on the set-up for EBFZM. Tungsten tubular feeds which were produced by CVD had an outer diameter of 16 mm and a wall thickness of 1.5 mm (a diameter of feeds varies from 10 to 22 mm). Seeds for growing single crystals were cut from the tubular cylindrical tungsten single crystals with the growth axis [111] and [001] by electroerosion, followed by removal of the damaged layer. Tubular crystals were grown in a vacuum higher than 10^{-4} Pa and at the rate of 4 mm min^{-1} . A special tubular holder for the tubular feed and single crystal was developed (Figure 13).

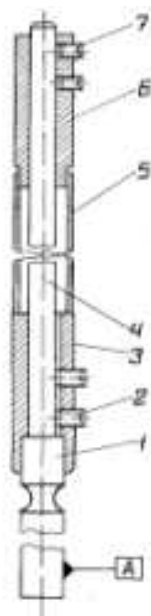


Figure 13. Device for growing tubular crystals.

The holder consists of the base 1, support shanks 3 and 6, the support rod 4, mounting screws 2 and 7. A small circular groove is performed on the base 1, through which it is possible quick and accurate align of the tubular feed. Since melting tubular feeds has some specific features, the relationship between the height of the liquid zone stability at EBFZM and the wall thickness is studied. Some proximity (blurring) of these two areas is possible due to the presence of destabilizing factors leading to local overheating in the zone: defects of cathode filament, oscillations of the impurity content in samples, as well as misalignment of the sample, cathode and focusing elements. A lower limit is due to the fact that an effect of the electron beam cutting is observed with increasing the current density of the electron beam. The obtained experimental dependence allows with sufficient reliability to pick up the electrical parameters of

melting using tubular specimens with the different diameters and wall thickness. In some cases, individual batches of feeds obtained by CVD have a high gas content which forced to resort to an additional step – the high-temperature vacuum annealing at pre-melting temperatures directly in the set-up. It turns out that without this preliminary operation the growth of tubular single crystals is impossible, since the escaping gases can tear off a liquid meniscus. A metallographic picture in Figure 14 shows the cross-section of the original CVD tubular feed after the above-described annealing operation (with partial melting). It shows also a clearly visible residual porosity. The assessment shows that for stable melting tubular feeds with a given wall thickness (from 0.5 to 1.5 mm) the zone height should be, respectively, from 2 to 4 mm. Naturally, these values meet the conditions of the focusing of the electron beam without local inhomogeneities in the density of the electron beam current.

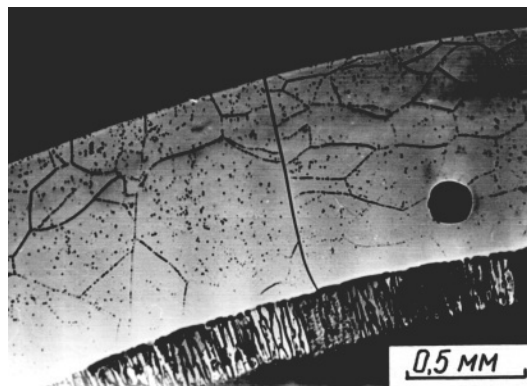


Figure 14. The cross-section of a tubular feed annealed.

The implementation of this condition is associated with great difficulties since it is necessary to supply large power to the tubular sample with a large radiating surface, which in turn affects the degree of superheating of the melt surface and the surface tension of the melt. Thus it is necessary to take into account the dependence of the stable zone height on superheating of the liquid metal, as well as decrease of viscosity of the liquid metal along with growing possibility of electron-beam cutting. Before the actual process of growing the tubular single crystal the radial heating by the filament of the electron gun should be carefully adjusted. The local density of the annular electron beam in either direction along the radius of no more than $\pm 20\%$ from the average current density, as shown in Figure 15.

When growing the tungsten tubular single crystals by seeding on a single crystalline seed of the desired crystallographic orientation, this operation is much more responsible than in the growth massive single crystals of cylindrical shape, since the presence of the slightest gap between the seed and the feed during welding them together can lead to rupture of the liquid meniscus. When growing tubular crystals without seeds, the grains from the base of the original CVD feed grow into the tubular crystal, and the high-angle boundaries tend to occupy the position of minimum energy, *i.e.*, they lie along the growth axis in diametrically opposite planes (Figure 16).

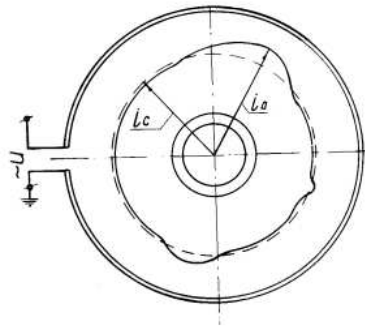


Figure 15. EB gun: optimal radial current density distribution.

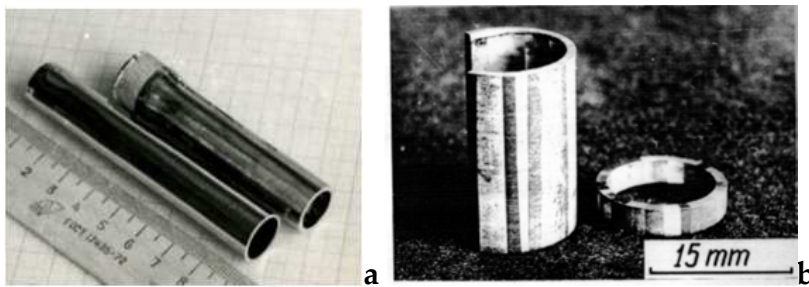


Figure 16. Single-crystalline (a) and polycrystalline (b) W tubes.

Thus obtained the polycrystalline tungsten tubes are very fragile and can be easily destroyed along the grain boundaries even from the weak strikes. When using the specially prepared single-crystal seeds it is possible to grow tubular single crystals of the length up to 180÷200 mm. The investigation of the real structure of the tubular single crystals of pure tungsten with the growth axes [111] and [001] is made by the metallographic and X-ray methods. In Figure 17 in the cross-section of the tubular single crystal, the low-angle boundaries are clearly seen, the majority of which begins and ends on the inner and outer surfaces of the tube.

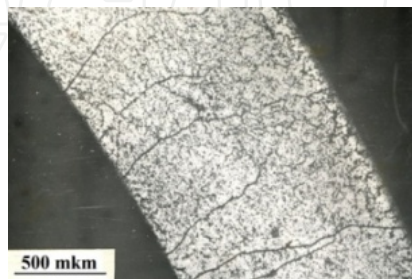


Figure 17. Low-angle boundaries in W tube crystal.

Subgrains originally contained in the seed have grown into a tubular single crystal, and their misorientation angles along the single crystal tend to be somewhat increased. A topogram of

angular scanning of the cross-section of the tubular tungsten single crystal with the growth axis [111] is shown in Figure 18.

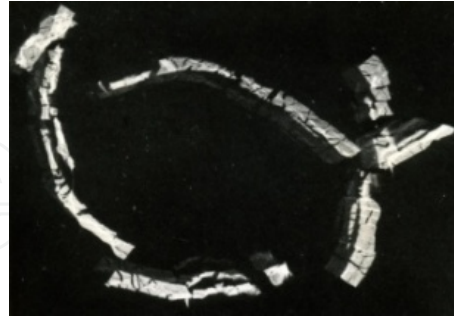


Figure 18. Topogram of angular scanning of a cross-section of W tube crystal.

In the cross-section, there are several large subgrains of first order, separated by low-angle boundaries with the misorientation angles less than $1\div 2^\circ$. Thus, the tungsten tubular single-crystals, obtained by EBFZM, at their crystallographic perfection are not inferior to the cylindrical tungsten single crystals obtained by the crystallization from the melt.

5.2. Features of capillary shaping in growing tubes

When growing single crystal at the initial portion of the tube at distances of about $(1.5\div 2)R_1$, where R_1 is the outer radius of an initial feed, there is a portion of unsteady growth. The radius of the growing crystal is continuously changed until a steady-state mode. Figure 19 shows the process of growing the tubular sample on the stationary phase.

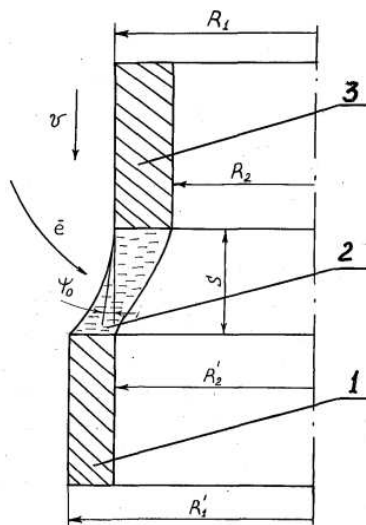


Figure 19. Growing a tubular W sample on the stationary phase: 1-feed, 2-meniscus, 3-tube crystal.

By solving Laplace equation of capillary the connection of the outer and inner radii of the growing tube crystal can be found. Forming the tube crystal would be stable if the capillary

constant a will be higher than the wall thickness [62], $\sigma = 2500 \text{ erg cm}^{-2}$ (the surface tension of the liquid W) and $a = \sqrt{2\sigma/\rho g} = 0.54 \text{ cm}$ (the capillary constant) [61]. In our case, the wall thickness of the initial feed is much less, and the fact that the height of the meniscus of the melt does not really exceed 3÷4 mm. So, it allows us, in a first approximation, to neglect by gravitational forces acting on the isothermal liquid meniscus. Using these simple limitations, it is possible to obtain connection between the initial tubular feed and the growing crystal. In a steady state the growth angle $\varphi_0 = \text{Const}$ and the tube crystal with a constant cross-section can grow. The mathematical profile description of the outer surface of the liquid meniscus is of considerable interest. Since the weight of the melt is neglected, then there is only a thin liquid film stretched between two rings with radii R_1' and R_1 , spaced at a distance of S (the height of the meniscus). Now, the profile of the meniscus can be found, if Laplace equation will be written in polar coordinates:

$$\partial^2 H / \partial r^2 + (1/r) (\partial H / \partial r) = 0 \quad (5)$$

with boundary conditions $H(r) |_{r=R_1} = 0; H(r) |_{r=R_1'} = S$. Problem is completely analogous to the problem of electrostatics for potential distribution within the cylindrical capacitor, so the solution of the equation after some simple transformations can be written as $H(r) = C \ln(r/R_1)$. Here, $S = C \ln(R_1'/R_1); C = S / \ln(R_1'/R_1)$. As a result, the surface profile to have a liquid meniscus equation:

$$H(r) = S / \ln(R_1'/R_1) \times \ln(r/R_1) \quad (6)$$

From which for the growth angle the equation can be written

$$\varphi_0 = \pi/2 - \text{arctg}(dH/dr |_{r=R_1}) \text{ or } \varphi_0 = \pi/2 - \text{arctg}[S / \ln(\frac{R_1'}{R_1}) \times (1/R_1)]. \quad (7)$$

The last equation can be written in a more convenient form:

$$S = \text{tg}(\pi/2 - \varphi_0) R_1 \ln R_1' \quad (8)$$

Since the growth angle φ_0 is a constant of material, the last equation gives an unambiguous link between the outer radius of the feed and the outer radius of the tubular crystal growing at a given height of the liquid meniscus S . The ratio for the tube inner radius R_2 is obtained from the law of mass conservation of (the difference between the density of the feed and the crystal, and evaporation losses are neglected)

$$R_2 = \sqrt{R_1^2 - (R_1')^2 + (R_2')^2} \quad (9)$$

The results of calculations are shown in Figure 20. It can be seen that the radius of the growing tubular crystal can be controlled by changing the height of the meniscus depending on the change of the electron beam power.

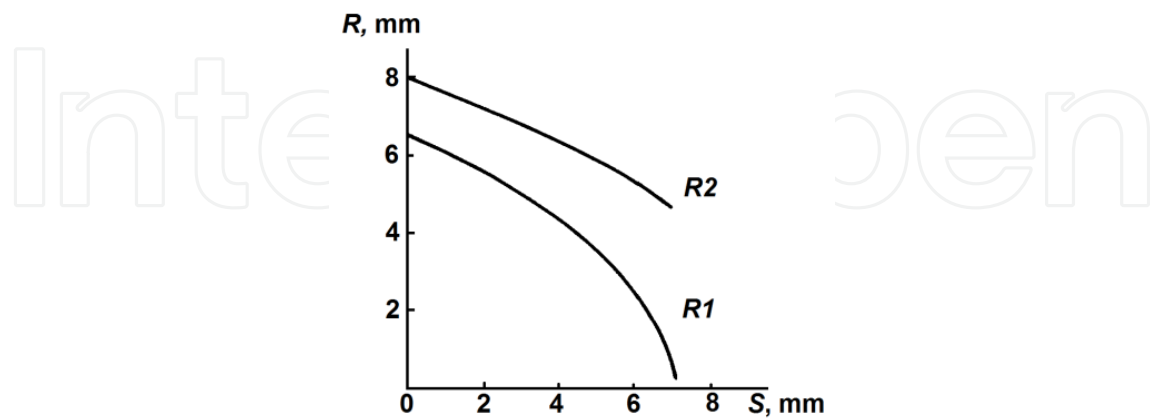


Figure 20. Dependence of radius of tube crystal on meniscus height.

The profile of the outer surface of the liquid meniscus is shown in Figure 21. According to measurements of the crystallized menisci the growth angle φ_0 is evaluated. For tungsten, it is found to be $20 \pm 5^\circ$, which is used in the calculations. It should be noted that in actual experiments, the height of the liquid meniscus S depends on many parameters: the initial feed geometry, thermal properties of material, power, focusing the electron beam, *etc.* In general, the quantity of S can be obtained by solving the experimental scheme of Stephen, but this is extremely difficult and hardly advisable. It should also be noted that the tungsten tubular single crystal grown by EBFZM have not only the high structural perfection, but also have even surfaces. The maximum height of the profile does not exceed ~ 100 microns. Shown that by EBFZM method the bicrystals with low-angle tilt and twist boundaries can be grown, and if the sub-boundary located in a plane parallel to the growth axis of the crystal grown, they can travel from the seed on considerable distances in the body of the crystal. Thus, the misorientation usually somewhat increases. This process takes place when low-angle boundaries in the given plane can be established by more or less complete combination of lattice dislocations.

It was shown that EBFZM method implemented at the new set-up, it is possible to grow single single-crystalline tungsten tubes of the high crystallographic and geometric perfection. This is due to the fact that the process of a capillary forming in the case, shown in Figure 19, has a high stability as repeatedly confirmed experimentally. Due to changes in the electron beam power it can be quite widely vary the height of the liquid meniscus S , *i.e.*, actually control of the diameter of the growing crystal. This gives us a hope that the process of growing single crystal tubes of refractory metals by EBFZM in perspective can be automatic that is particularly necessary in the case of the serial production of such products. Currently, the process of growing tubes by an operator control, which actually measures the relevant parameters: the meniscus height S and diameter of the growing tubular crystal $2R_1$ "by eye", which is totally

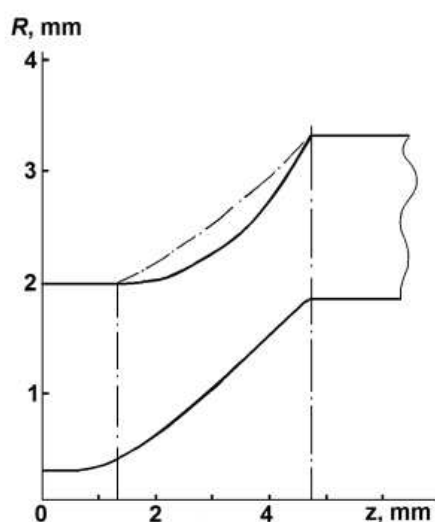


Figure 21. Inner and outer profiles in the feed-melt-crystal system.

inadequate in the sense of obtaining single-crystal tubes of specified geometrical sizes. Furthermore, if the growth process is in a stationary stage, and power of the electron beam with a high accuracy ($\pm 0.5\%$ for setting "area") is maintained at a constant preset level, it does not mean that the crystal will grow of a constant cross-section. The shank and the free end of the tubular feed influence on the heat transfer from the liquid meniscus portion. As a result of change of the meniscus height S , and hence change of the diameter of the growing crystal is happened. The latter leads to presence in the tubular single crystal tapers of both signs. This is clearly seen in Figure 22. Obviously, the taper can be eliminated by an automatic control system of the growth process. For example, in growing single crystals of semiconductor materials by Czochralski or Stepanov such automatic systems are already widely used [7]. It should be noted that such a process parameter to measure the height of the meniscus is in any way unlikely. Measuring the diameter of the growing crystal is possible by means of an optical system or a TV monitor. The resulting signal from the sensor of the diameter is then used to synthesize an appropriate control signal to an analog control unit or microcomputer. One of the important parameters of the automatic control system is its speed. Obviously, in the case of growing tubes by EBFZM this value should be much smaller than the thermal time constant of the thermal process zone (the crystal plus the corresponding accessories). Since, as previously shown, the taper is mostly due to change of heat removal by conduction, it is possible to obtain the following estimate for the time constant of the form: $\tau = Q/\chi$, where, χ the thermal diffusivity, $\text{cm}^2 \text{s}^{-1}$; Q the cross-section of the crystal, cm^2 . For the tungsten tubular single crystal with the outer diameter of 16 mm, the wall thickness $\delta = 2$ mm and the registered thermal time constant yields to $\tau = 4$ s. Therefore, the creation of ACS for growing tubes by EBFZM with the rate much less than 4 s do not represent currently any technical difficulties. The system would eliminate defects like geometric tapers and grow single crystalline tubes of refractory metals by EBFZM with a deviation of the inner and outer diameters from the nominal value within ± 200 microns, and getting these products on an industrial scale.

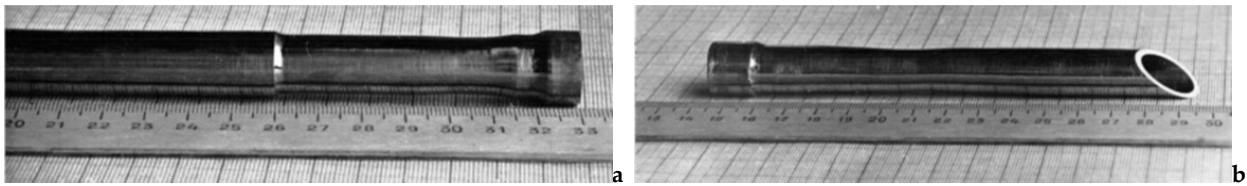


Figure 22. W tubular single crystals with a growth axis [111], comprising one-two runs (a) and a tapering defect in the middle (b).

6. Key findings

1. The method is developed of growing bicrystals of refractory metals up to 150-200 mm in diameter and 15-25 mm with the desired crystallographic parameters - of misorientation angles and both the grain boundaries and bedding planes of boundaries. The method is based on stability and radial uniformity of power supplied to the sample by an electron gun, co-axiality of the growing bicrystal and the electron gun, and the uniformity of heat removal from the growing bicrystal. Proposed and tested three methods of preparing bicrystalline seeds allow to grow bicrystals of niobium, molybdenum and tungsten with crystallographic parameters within $1-2^\circ$. Shown that by EBFZM method can be grown the bicrystals with desired low-angle tilt and twist boundaries, and if sub-boundary is located in a plane parallel to the growth axis of the crystal grown, they can travel from the seed on considerable distances in the body of the crystal. Thus the misorientation usually somewhat increases. This process takes place when the small-angle boundary in the given plane can be established by more or less complete combination of lattice dislocations. It is shown that a new set-up meets the most stringent requirements to the electron-beam zone melting set-ups for the radial uniformity of heating, power stability, and production efficiency.
2. The thirty-years experience of growing single crystals, bicrystals, and tubular crystals with desired crystallographic parameters and geometry have shown that the developed EBFZM set-ups together with new electron-beam guns are of the successful design. They give an excellent possibility to grow any of single-crystalline samples of transition metals of diameter from 4 to 30 mm. These opportunities are determined primarily by the original circular electron guns for growing crystals of different diameters. The electron guns themselves have no restrictions in duration of their work and life and are essentially "eternal". Single crystals grown of all studied transition metals satisfy the highest requirements for both the chemical purity and structural perfection. Duration of the circular tungsten cathodes made of tungsten wire with a diameter of 0.8-1 mm is longer than 100 hours. Growing crystals up to 600 mm long is provided by the design of EBFZM set-ups. The main principle of designing the set-ups is the co-axiality of the cathode and anode assemblies throughout the whole length of the growing crystal. In other words, the geometric and thermal centers of the crystal and the melt should be matched, as well as

high precision of moving mechanisms of both the anode and cathode assemblies and offset buckling and vibration as result of thermal effects.

3. Proposed and tested three methods of preparing bicrystalline seeds to grow bicrystals with controlled crystallographic parameters of high accuracy (up to $1-2^\circ$). The fracture strength of high-angle tilt and twist boundaries in the pure molybdenum bicrystals is low; special boundaries differ markedly from other boundaries on their strength: twin boundaries are several times stronger and boundaries with small numbers of coincident nodes have the lowest strength. The contents of interstitials at boundaries of high-angle misorientation, according to Auger electron spectroscopy, almost tenfold higher than their content in the grain volume. However, increasing the purity of molybdenum on interstitials does not lead to change in the fracture strength of grain boundaries. Shown that by EBFZM method can be grown bicrystals with low-angle tilt and twist boundaries.
4. Our results have shown that the combination of bicrystalline samples and low-energy ions scattering (LEIS) is very fruitful. The experimental results show that using bicrystals in combination with LEIS opens new possibilities for studying properties of surfaces. Experimentally shown that the LEIS signal intensity from the different crystallographic surfaces of molybdenum bicrystals is defined by both the atomic density of the uppermost atomic layer and its structure. Contributions of second and deeper layers in the LEIS signal are very small (<2%). After bombardment by the Ne^+ ions with energy of 3 keV and different ion doses (from 7×10^{15} to 4×10^{16} ion cm^{-2}) with current of 6×10^{12} ion $\text{cm}^{-2} \text{c}^{-1}$, the difference between the LEIS signal intensities for molybdenum planes Mo(110) and Mo(100) remain at 10%, indicating partial damage of the surface. Rather, at such ion fluxes sputtering the surfaces occurs layer-by-layer. Our studies have shown that the processes can also be examined using the self-diffusion method of LEIS as the LEIS signal may be to some extent an indication of damage of the surface. Using this method the study of properties of the surface recrystallization can also be conducted. We have found that recrystallization of molybdenum surface Mo(110) begins at 750°C and of $\sim\text{Mo}(100)$ - at about 1300°C , indicating the different mobility of atoms in the uppermost atomic layers of different crystallographic orientations surface. Moreover, the LEIS signal intensity of the surface Mo(110) during sputtering drops to 75% of its initial level (for a clean surface free of damage), and of Mo(100) - to 90% only. It follows that the close-packed surface structure is more sensitive to these influences, which may be attributed to its low free energy.
5. The growing technology of tubular tungsten single crystals by EBFZM is developed. It is shown that capillary shaping of the tube crystals is stable. A crystallographic perfection of tungsten tubular single crystals is not inferior to the cylindrical single crystals, obtained by EBFZM. This is due to the fact that capillary forming is of high stability what is confirmed experimentally. Due to changes in power the height of the liquid meniscus can be widely varied what is very important to check the diameter of growing tubular crystals. This gives a hope that growing single crystalline tubes of transition metals by EBFZM can be automatic in perspective.

Acknowledgements

I want to express my acknowledgments to my colleagues and friends Boris Shipilevsky, Valery Semenov, Sergey Bozhko, Eugene Stinov, and Sergey Markin from ISSP RAS for the long cooperation in my life and science. I am very grateful to Hidde Brongersma, Honorary Professor of Physics of Technical University Eindhoven and Imperial College London, for fruitful discussions and cordial friendliness during many years of our life. I am very grateful to Victor Lomeyko, ISSP RAS, for his skillful engineering assistance at the most part of my scientific studies. I have to express my acknowledgments to the Russian Fund for Basic Research for financial support of the part of these studies.

Author details

Vadim Glebovsky*

Address all correspondence to: glebovs@issp.ac.ru

Institute of Solid State Physics, the Russian Academy of Sciences, Russia

References

- [1] Chernov A.A., Givargizov E.I., Bagdasarov H.S., Kuznetsov V.A., Demyanetz P.N., Lobachev A.N. *The Contemporary Crystallography*. Moscow: Nauka, 1980.
- [2] Laudise, R. A., Parker R.L. *The Growth of Single Crystals*. Moscow: Mir, 2010.
- [3] Parker, R. L. *Crystal Growth Mechanisms: Energetics, Kinetics and Transport*. New York: Academic, 1970.
- [4] Ullhoff M.K. Shape and Stability of Menisci in Czochralski Growth and Comparison with Analytic Approximation. *Journal of Crystal Growth* 1975;30(1) 9-20. DOI: 10.1016/0022-0248(75)90192-X.
- [5] Hurle D.T. Control of Diameter in Czochralski and Related Crystal Growth Techniques. *Journal of Crystal Growth* 1977;42 473-482. DOI: 10.1016/0022-0248(77)90233-0.
- [6] Langer J.S. Instabilities and Pattern Formation in Crystal Growth. *Revue of Modern Physics* 1980;52(1) 1-28.
- [7] Savitsky E.M., Burkhanov G.S. Growth of Single Crystals of High Melting Metal Alloys and Compounds by Plasma Heating. *Journal of Crystal Growth* 1978; 43(4) 616-624. DOI: 10.1016/0022-0248(78)90343-3.
- [8] Pfann W.G. *Zone Melting* (2nd Edition), New York, 1966.

- [9] Tiller W.A. *The Science of Crystallization: Macroscopic Phenomena and Defect Generation*, Cambridge University Press, 1991. ISBN 978-0-521-38828-3.
- [10] Tiller W.A. *The Science of Crystallization: Microscopic Interfacial Phenomena*, Cambridge University Press; 1991. ISBN 978-0-521-38827-6.
- [11] Buckley-Golder J.M., Hurphreys C.J. Theoretical Investigation of Temperature Distribution during Chochralski Crystal Growth. *Philosophical Magazine* 1979; 39(1) 41-57. DOI:10.1080/01418617908239274.
- [12] Kobayashi N. Power Required to Form a Floating Zone and the Zone Shape. *Journal of Crystal Growth* 1978; 43(4) 417-424. DOI: 10.1016/0022-0248(78)90339-1.
- [13] Kobayashi N., Wilcox W.C. Computational Studies of Convection in a Cylindrical Floating Growth. *Journal of Crystal Growth* 1982; 59(3) 616-624. DOI: 10.1016/0022-0248(82)90385-2.
- [14] Wilcox W.R., Fuller L.D. Turbulent Free Convection in Czochralski Crystal Growth. *Journal of Applied Physics* 1965;36 2201-2205.
- [15] Barthel J. Hydrodynamics of the Melt in Zone Floating and its Influence on Single Crystal Perfection. In: *ISSCG-4, Moscow, 1980*;1: p203-267.
- [16] Dash W.C. Silicon Crystals Free of Dislocations. *Journal of Applied Physics* 1958; 29: 736-737.
- [17] Nes E., Most W. Dislocation Densities in Slow Cooled Aluminum Single Crystals. *Philosophical Magazine* 1966;13(124) 855-859.
- [18] Akita H., Sampare D.S., Flore N.F. Substructure Control by Solidification Control in Copper Crystals. *Metallurgical Transactions* 1973;4 1593-1597.
- [19] Cole M., Fisher D.S., Bucklow J.A. Improved Electron Beam Device for Zone Melting. *British Journal of Applied Physics* 1961;12(10) 577-578.
- [20] Glebovsky V. *Crystal Growth: Substructure and Recrystallization*. In: *Recrystallization*, Ed. K. Sztwiertnia, Rieka: InTech, 2012. ISBN 978-953-51-0122-2.
- [21] Glebovsky V.G., Lomeyko V.V., Semenov V.N. Unit for Electron-beam Zone Melting of Refractory Materials. *Journal of Less-Common Metals* 1986;117 385-389. DOI: 10.1016/0022-5088(86)90064-0.
- [22] Glebovsky V.G., Semenov V.N., Lomeyko V.V. Influence of the Crystallization Conditions on the Structural Perfection of Molybdenum and Tungsten Single Crystals. *Journal of Crystal Growth* 1988; 87(1) 142-150. DOI:10.1016/0022-0248(88)90353-3.
- [23] Glebovsky V.G., Kopetsky C.V., Myshlyaev M.M., Romanov Y.A. Steady-state Creep and Dislocation Structure of Molybdenum. *Physics of Metals & Metallography* 1976;41(3) 150-158.

- [24] Myshlyaev M.M., Romanov Y.A., Senkov O.N., Khodos I.I., Glebovsky V.G. High Temperature Creep and Dislocation Structure in Tungsten Single Crystals. *Problemy Prochnosti* 1979;5 26-34.
- [25] Aristov V.V., Shmytko I.M., Shulakov E.V. Application of the X-ray Divergent-beam Technique for the Determination of the Angles between Crystal Blocks. I. Reflexion from the planes parallel to the crystal surface. *Journal of Applied Crystallography* 1974; 7(4) 409-413. doi:10.1107/S0021889874010028.
- [26] Fromm E., Gebhardt E. *Gase und Kohlenstoff in Metallen*. Berlin. 1976.
- [27] Glebovsky V.G., Kazantsev A.M., Pronman I.M., Shipilevsky B.M. Investigation of oxygen distribution in Nb single crystals by the method of fast-neutron activation. *Physics of Metals & Metallography* 1980;49(3) 130-136.
- [28] Glebovsky V.G., Kapchenko I.V., Kireyko V.V., Oblivantsev A.N., Rybasov A.G. The behaviour of Oxygen and Carbon in the Process of Electron Beam Zone Melting of Niobium. *Journal of Crystal Growth* 1986;74(3) 529-534. DOI: 10.1016/0022-0248(86)90198-3.
- [29] Gantmacher V.F., Petrashev V.T. Scattering of Conduction Electrons on Pure Metals. In: *Metals of High Purity*. Moscow: Nauka, 1976; 31-35.
- [30] Gust W., Hirtz M.B., Predel B., Roll U. Techniques for the Production of Oriented Bicrystals and Results on Specimens Prepared by these Methods. *Acta Metallurgica* 1980; 28(9) 1235-1244.
- [31] Yastrebkov A.A., Ivakin Y.P. Influence of the Misorientation Angle on Strength of Intergranular Boundaries of Molybdenum. *Physics of Metals & Metallography* 1975; 40(3) 594-598.
- [32] Clough S.P., Vonk S.J., Stein D.F. Preparation of Oriented Molybdenum Twist Boundaries by Electron-beam Zone Melting. *Journal of Less-Common Metals* 1976; 50(1) 161-163.
- [33] Liu J.M., Shen W.-W. Grain Boundary Fracture in Tungsten Bicrystals. *Acta Metallurgica* 1982; 30(6) 1197-1202.
- [34] Glebovsky V.G., Sursaeva V.G., Semenov V.N. The Strength of Individual Grain Boundaries of High Purity Molybdenum. In: *Int. High Purity Materials in Science and Technology*, Dresden, 1985, p.337-338.
- [35] Cai B.C., Dasgupta A., Chou Y.T. A New Technique for the Growth of Bicrystals of Refractory Metals. *Journal of Less-Common Metals* 1982;86 145-151.
- [36] Pande C.S., Lin L.S., Bulter S.R., Chou Y.T. Use of Floating Zone Melting Technique for the Growth of Niobium Bicrystals. *Journal of Crystal Growth* 1973;19(5) 209-210. DOI: 10.1016/0022-0248(73)90112-7.

- [37] Glebovsky V.G., Moskvina S.I., Semenov V.N. Growing Techniques and Structure of Niobium Bicrystals. *Journal of Crystal Growth* 1982;59 450-454. DOI: 10.1016/0022-0248(82)90366-9.
- [38] Brehm W.P., Gregg I.L. Growth of Oriented Nb Bicrystals by Arc-Zone Melting. *Journal of Less-Common Metals* 1968;14 463- 465. DOI: 10.1016/0022-5088(68)90171-9.
- [39] Brosse J.B., Fillard R., Biscondi M. Intrinsic Intergranular Brittleness of Molybdenum. *Scripta Metallurgica* 1981;15(6) 619-623.
- [40] Kobylanski A., Goux C. Sur la Fragilite Intergranulaire du Molybdene Etudiee l'aide de Bicristaux de Flexion Symetrique autmur de Laxe [001]. *C.R.Acad.Sc.Paris* 1971;272(C) 1937-1940.
- [41] Reid C.N. Dislocation Widths in Anisotropic bcc Crystals. *Acta Metallurgica* 1966;14 13-16.
- [42] Kurishita H., Yoshinaga A. The Strength of Grain Boundary in Molybdenum. *Japan Materials Science, Japan* 1980;17 239-240.
- [43] Kumar A., Eyre B.L. Grain Boundary Segregation and Intergranular Fracture in Molybdenum. *Progress of Royal Society A, London* 1980;370 431-458.
- [44] V.G. Sursaeva, V.G. Glebovsky, V.N. Semenov, C.V. Kopetsky, Y.M. Shulga, L.S. Shvindlerman. Strength of Intergranular Tilt and Twist Boundaries in Molybdenum Bicrystals. *Physics of Metals & Metallography* 1985;59(4) 166-173.
- [45] Vinnikov L.Y., Glebovsky V.G., Moskvina S.I. Vortex Pinning in Nb Bicrystals. *JETP Letters* 1981;33 239-243.
- [46] Glebovsky V.G., Lomeyko V.V., Moskvina S.I., Semenov V.N., Vinnikov L.Y. Growth and Structure of Niobium Bicrystals. *Physics of Metals & Metallography* 1982;54(4) 137-140.
- [47] V.G. Sursaeva, V.G. Glebovsky, Y.M. Shulga, L.S. Shvindlerman. Strength of Individual Special Tilt and Twist Boundaries in Molybdenum Bicrystals. *Scripta Metallurgica* 1985;19 411-414.
- [48] Mishlyaev M.M., Khodos I.I., Senkov O.N., Romanov Y.A. Features of Dislocation Structure of Interblock Boundaries in bcc Single Crystals. *Physics of Metals & Metallography* 1980; 48(1) 148-157.
- [49] Yastrebkov A.A., Ivakin Y.P. Influence of Misorientation Angle on Brittleness of Tungsten Bicrystals. *Physics of Metals & Metallography* 1973;36 135-139.
- [50] Sosnina E.I., Matvienko L.F., Meleshko L.I. Growth anisotropy of misorientations and the symmetry of substructure boundaries in alloyed single crystals of molybdenum and tungsten. *Physics of Metals* 1981;3(2) 101-110.

- [51] Ermolov S.N., Jansen W.P.A., Markin S.N., Glebovsky V.G., Brongersma H.H. Surfaces of Mo Bicrystals Studied by Low Energy Ion Scattering. *Surface Science* 2002;512 221-228. DOI: 10.1016/S0039-6028(02)01663-1
- [52] Ermolov S.N., Glebovsky V.G., Jansen W., Markin S.N., Brongersma H.H. Study of Mo Bicrystals by Low Energy Ion Scattering. *Izvestiya RAS, Fizicheskaya Seriya* 2002;66(4) 580-585.
- [53] Sutton A.P., Baluffi R.W. *Interfaces in Crystalline Materials*. Oxford: Clarendon Press, 1995.
- [54] Cortenraad R., Ermolov S.N., Moest B., A.W. Denier van der Gon, Glebovsky V.G., Brongersma H.H. Crystal Face Dependence of Low Energy Ion Scattering Signals. *Nuclear Instruments & Methods in Physics Research B* 2001;174(1-2) 173-180. DOI: 10.1016/S0168-583X(00)00452-3.
- [55] Cortenraad R., A.W. Denier van der Gon, Brongersma H.H., Ermolov S.N., Glebovsky V.G. On the Quantification of the Surface Composition of Low Work Function Surfaces Using Low Energy Ion Scattering. *Surface & Interface Analysis* 2001;31 (3) 200-205. DOI: 10.1002/sia.972.
- [56] Bergmans R.H. *Energy and Angle Resolved Ion Scattering and Recoiling Spectroscopy on Bimetallic Systems*. PhD Thesis. Eindhoven University of Technology, Eindhoven, The Netherlands, 1996. ISBN 90-386-0057-7.
- [57] Glebovsky V.G., Semenov V.N., Lomeyko V.V. Peculiarities of the Growth and Structure of Pure Tungsten Tubular Polycrystals and Single Crystals. *Visokochistie Veshchestva (High Purity Materials)* 1988;5 37-41.
- [58] Glebovsky V.G., Semenov V.N., Lomeyko V.V. The Characteristic Features of Growth and the Real Structure of Tungsten Tube Crystals. *J. Crystal Growth* 1989;98(2) 487-491. DOI: 10.1016/0022-0248(89)90165-6.
- [59] Glebovsky V.G., Semenov V.N., Lomeyko V.V. On the Problem of Growing Tungsten Single-Crystalline Tubes from the Melt. *Vacuum* 1990;41 2165-2166. DOI: 10.1016/0042-207X(90)94214-B.
- [60] Surek T, Cornell S.R., Chalmers B. The Growth of Shaped Crystals from the Melt. *Journal of Crystal Growth* 1980;50(1) 21-32. DOI: 10.1016/0022-0248(80)90227-4
- [61] Fogel A.A. *HF Induction Levitation of Liquid Metals*. Leningrad: Mashinostroenie. 1989.
- [62] Eriss I., Stormont R.W., Surek T., Taylor A.S. The Growth of Silicon Tubes by EFG process. *Journal of Crystal Growth* 1980;50(1) 200-211. DOI: 10.1016/0022-0248(80)90244-4.